Monthly Notices
of the
ROYAL ASTRONOMICAL SOCIETY

Mon. Not. R. Astron. Soc. **400,** 273–290 (2009) doi:10.1111/j.1365-2966.2009.15448.x

Probing the near-infrared stellar population of Seyfert galaxies

R. Riffel,[1]★ M. G. Pastoriza,[1] A. Rodríguez-Ardila[2]† and C. Bonatto[1]

[1]*Departamento de Astronomia, Universidade Federal do Rio Grande do Sul. Av. Bento Gonçalves 9500, Porto Alegre, RS, Brazil*
[2]*Laboratório Nacional de Astrofísica/MCT - Rua dos Estados Unidos 154, Bairro das Nacões, Itajubá, MG, Brazil*

Accepted 2009 July 23. Received 2009 June 5; in original form 2008 December 19

ABSTRACT

We employ Infrared Telescope Facility SpeX near-infrared (NIR; 0.8–2.4 μm) spectra to investigate the stellar population (SP), active galactic nuclei (AGN) featureless continuum (FC) and hot dust properties in nine Sy 1 and 15 Sy 2 galaxies. Both the STARLIGHT code and the hot dust as an additional base element were used for the first time in this spectral range. We found evidence of correlation among the equivalent widths (W_λ) Si I 1.59 μm × Mg I 1.58 μm, equally for both kinds of activity. Part of the $W_{\rm Na\,I\,2.21\,\mu m}$ and $W_{\rm CO\,2.3\,\mu m}$ strengths may be related to galaxy inclination. Our synthesis shows significant differences between Sy 1 and Sy 2 galaxies: the hot dust component is required to fit the *K*-band spectra of ∼90 per cent of the Sy 1 galaxies, and only of ∼25 per cent of the Sy 2; about 50 per cent of the Sy 2 galaxies require an FC component contribution $\gtrsim$20 per cent, while this fraction increases to about 60 per cent in the Sy 1; also, in about 50 per cent of the Sy2, the combined FC and young components contribute with more than 20 per cent, while this occurs in 90 per cent of the Sy1, suggesting recent star formation in the central region. The central few hundred parsec of our galaxy sample contain a substantial fraction of intermediate-age SPs with a mean metallicity near solar. Our SP synthesis confirms that the 1.1 μm CN band can be used as a tracer of intermediate-age SPs. The simultaneous fitting of SP, FC and hot dust components increased in ∼150 per cent the number of AGNs with hot dust detected and the mass estimated. The NIR emerges as an excellent window to study the SP of Sy 1 galaxies, as opposed to the usually heavily attenuated optical range. Our approach opens a new way to investigate and quantify the individual contribution of the three most important NIR continuum components observed in AGNs.

Key words: stars: AGB and post-AGB – circumstellar matter – infrared: stars.

1 INTRODUCTION

A key issue in modern astrophysics is to understand the origin of the energy source that powers the continuum and line-emitting gas in active galactic nuclei (AGN). The current paradigm proposes that accretion of material on to a supermassive black hole located at the centre of the galaxy is the mechanism responsible for the observables associated with the AGN phenomena. In addition to this central engine, observational evidence over the past decade has shown that massive star-forming regions are commonly detected in the central region of galaxies harbouring an AGN (e.g. Tokunaga et al. 1991; Mizutani, Suto & Maihara 1994; Imanishi & Dudley 2000; Storchi-Bergmann et al. 2000; Imanishi 2002; Rodríguez-Ardila & Viegas 2003; Riffel et al. 2007; Dors et al. 2008). In this scenario, black holes and starburst clusters coexist in the nuclear region of galaxies. Currently, there is ample evidence indicating that both the active nucleus and starburst might be related to gas inflow, probably triggered by an axis-asymmetry perturbation like bars, mergers or tidal interactions (Shlosman, Frank & Begelman 1989; Shlosman, Begelman & Frank 1990; Maiolino et al. 1997; Knapen, Shlosman & Peletier 2000; Fathi et al. 2006; Riffel et al. 2008a), providing support to the so-called AGN–starburst connection (Norman & Scoville 1988; Terlevich, Diaz & Terlevich 1990; Heckman et al. 1997; Cid Fernandes 1997; González-Delgado et al. 1998; Veilleux 2000; Ferrarese & Merritt 2000; Heckman 2004; Riffel et al. 2008a, and references therein).

Another line of thought, however, claims that this AGN–starburst connection could be incidental, as many Seyferts do not show any evidence of starburst activity (e.g. Filippenko, Ho & Sargent 1993), and optical spectroscopic studies of large samples do not indicate that starbursts are more common in Seyferts than in normal

★E-mail: riffel@ufrgs.br
†Visiting Astronomer at the Infrared Telescope Facility, which is operated by the University of Hawaii under Cooperative Agreement no. NCC 5-538 with the National Aeronautics and Space Administration, Office of Space Science, Planetary Astronomy Program.

galaxies (Pogge 1989). In addition, Cid Fernandes et al. (2004, hereafter CF04) studied the optical stellar population (SP) of 65 Sy 2 and 14 other galaxies from the Joguet et al. (2001) sample. They concluded that the star formation history (SFH) of the Sy 2 galaxies is remarkably heterogeneous. These results are similar to those obtained in the study of the UV and optical SP of Seyfert galaxies (mostly Sy 2) available in the literature (e.g. Bica 1988; Schmitt, Bica & Pastoriza 1996; Cid Fernandes, Storchi-Bergmann & Schmitt 1998; González-Delgado et al. 1998b; Bonatto et al. 2000; Raimann et al. 2003; González-Delgado et al. 2004; Cid Fernandes et al. 2005b, CF04, and references therein).

To determine if circumnuclear SPs and nuclear activity are closely related phenomena, or if they are only incidental, it is of utmost importance for the correct characterization of the former, since a substantial fraction of the energy emitted by a galaxy in the optical-to-near-infrared (NIR) domain is starlight. Moreover, the analysis of the stellar content provides information on critical processes such as the star formation episodes and the evolutionary history of the galaxy. In this respect, the use of NIR features in the study of SP is not recent, dating back to nearly three decades ago. For example, Rieke et al. (1980) employed NIR spectroscopy to study NGC 253 and M82. They report the detection of a strong 2.2 μm CO band, suggesting the presence of a dominant population of red giants and supergiants in the nuclear region of both sources. Since then, other authors have used the NIR to study star formation, in most cases based on the 2.2 μm CO band (e.g. Origlia, Moorwood & Oliva 1993; Oliva et al. 1995; Engelbracht et al. 1998; Lançon et al. 2001, and references therein) or photometric methods (e.g. Moorwood & Glass 1982; Hunt, Thuan & Izotov 2003).

One reason to use the NIR to study the SP of AGNs is that it is the most convenient spectral region accessible to ground-based telescopes to probe highly obscured sources. However, tracking the star formation in the NIR is complicated (Origlia & Oliva 2000). Except for a few studies such as those based on the Brγ emission or the CO(2–0) first overtone (e.g. Origlia et al. 1993; Oliva et al. 1995), the SP of the inner few hundred parsec of active galaxies in the NIR remains poorly known. Because stellar absorption features in the NIR are widely believed to provide a means for recognizing red supergiants (Oliva et al. 1995), they arise as prime indicators for tracing starbursts in galaxies. Besides the short-lived red supergiants, the NIR also includes the contribution of thermally pulsating asymptotic giant branch (TP-AGB) stars, enhanced in young-to-intermediate-age SPs ($0.2 \leq t \leq 2$ Gyr; Maraston 1998, 2005). The TP-AGB phase becomes fully developed in stars with degenerate carbon oxygen cores (see Iben & Renzini 1983, for a review). Evidence of this population in the optical is usually missed, as the most prominent spectral features associated with this population fall in the NIR (Maraston 2005).

With the new generations of Evolutionary Population Synthesis (EPS) models, which include a proper treatment of the TP-AGB phase (Maraston 2005), it is now possible to study in more detail the NIR SP of galaxies. According to these models, the effects of TP-AGB stars in the NIR spectra are unavoidable. Maraston (2005) models, by including empirical spectra of oxygen-rich stars (Lançon & Wood 2000), are able to foresee the presence of NIR absorption features such as the 1.1 μm CN band (Riffel et al. 2007), whose detection can be taken as unambiguous evidence of a young-to-intermediate-age SP.

Given the above, we feel motivated to carry out the first detailed study of the SP in active galaxies in the NIR using the entire 0.8–2.4 μm spectral range. This paper is structured as follows: the data are presented in Section 2. NIR spectral indices are presented in Section 3. In Section 4 we describe the fitting method. Results are presented and discussed in Section 5. The final remarks are given in Section 6.

2 THE DATA SET

We chose for this work a subsample of 24 from the 47 AGNs with NIR spectra published by Riffel, Rodríguez-Ardila & Pastoriza (2006). The selected targets display prominent absorption lines/bands and are listed in Table 1. All spectra were obtained at the NASA 3-m Infrared Telescope Facility (IRTF). The SpeX spectrograph (Rayner et al. 2003) was used in the short cross-dispersed mode (SXD, 0.8–2.4 μm). The detector used was a 1024 × 1024 ALADDIN 3 InSb array with a spatial scale of 0.15 arcsec pixel^{-1}. A 0.8 × 15 arcsec^2 slit was employed giving a spectral resolution of 360 km s^{-1}. The radius of the central integrated region is a few hundred parsec for almost all sources.[1] For more details on the instrumental configuration, data reduction, calibration processes and integrated region, see Riffel et al. (2006). A rapid inspection of figs 9, 10 and 12 in Riffel et al. (2006) shows that all the chosen spectra are dominated by strong absorption features, the most prominent ones are identified in fig. 1 of Riffel et al. (2008b).

3 NEAR-INFRARED SPECTRAL INDICES: DIRECT MEASUREMENTS

For comparison with published works and future NIR SP studies, we compute the equivalent widths (W_λ) of the NIR absorption features as well as selected continuum fluxes (F_λ) in regions free from emission/absorption, normalized to unity at 1.223 μm. W_λ and F_λ are measured according to the definitions of Riffel et al. (2008b). The values of W_λ and F_λ are presented in Tables 1 and 2, respectively.

The most studied absorption lines in the literature and present in our spectral range are the calcium triplet lines (CaT,[2] e.g. Terlevich et al. 1990; Garcia-Rissmann et al. 2005; Vega et al. 2009, and references therein).

We have four of our objects (Mrk 573, Mrk 1066, NGC 2110 and Mrk 1210) in common with Vega et al. (2009). For the first three objects we measure values larger than those reported by them. The difference is due to the different index definitions. While we use those of Bica & Alloin (1987), Vega et al. (2009) use Cenarro et al. (2001). The CaT in Mrk 1210 occurs near the detection limit in our spectrum, which thus preclude measurements. Vega et al. (2009) report a value of 6.22 ± 0.48 Å for this feature. In addition, the differences between our measurements and those of Vega et al. (2009) can be related to the fact that they measure $W_{\rm CaT}$ in their synthetic spectra, and therefore our measurements represent better the conditions observed in actual galaxy spectra. Other explanation for the discrepancies probably lies in the different apertures used in both works. They use a slitwidth of 2.0 arcsec (Garcia-Rissmann et al. 2005) while we use a slit 2.5 times narrower (Riffel et al. 2006). Terlevich et al. (1990) report CaT measurements for NGC 3227, NGC 262 (Mrk 348) and NGC 5953. Our $W_{\rm CaT}$ value for the former is consistent with theirs, while for the latter two we measure higher values. The discrepancy is again due to the different continuum

[1] Lower than 300 pc for 15 objects, between 300 and 500 pc for six and >500 for three. For more details, see column 10 of table 1 of Riffel et al. (2006).

[2] $W_{\rm CaT} = W_{\rm CaT1\,0.849\,\mu m} + W_{\rm CaT2\,0.854\,\mu m} + W_{\rm CaT3\,0.867\,\mu m}$.

Table 1. Equivalent widths measured in the galaxy sample (in Å).

Object/ion	CaT$_1$	CaT$_2$	CaT$_3$	CN	Al I	Na I	Si I	Mg I	Si I	CO	Na I	Ca I	CO	CO	CO
BP$_b$(μm)	0.8476	0.8520	0.8640	1.0780	1.1200	1.1335	1.2025	1.5720	1.5870	1.6110	1.1936	2.2570	2.2860	2.3150	2.3420
BP$_r$(μm)	0.8520	0.8564	0.8700	1.1120	1.1300	1.1455	1.2200	1.5830	1.5940	1.6285	2.2150	2.2740	2.3100	2.3360	2.3670
centre(μm)	0.8498	0.8542	0.8670	1.0950	1.1250	1.1395	1.2112	1.5771	1.5894	1.6175	2.2063	2.2655	2.2980	2.3255	2.3545
(1)	(2)	(3)	(4)	(5)	(6)	(7)	(8)	(9)	(10)	(11)	(12)	(13)	(14)	(15)	(16)
Seyfert 2															
NGC 262(‡)	3.82 ± 0.44	5.92 ± 0.44	4.11 ± 0.42	-	-	-	-	1.41 ± 0.27	2.17 ± 0.05	-	1.04 ± 0.04	-	2.75 ± 0.01	0.74 ± 0.03	1.78 ± 0.02
Mrk 993	1.41 ± 0.15	3.46 ± 0.13	2.73 ± 0.12	-	-	2.57 ± 0.01	-	3.58 ± 0.13	2.22 ± 0.05	2.43 ± 0.04	3.03 ± 0.04	-	9.04 ± 0.01	5.24 ± 0.03	8.34 ± 0.03
NGC 591	5.80 ± 0.39	4.57 ± 0.29	4.72 ± 0.17	16.95 ± 0.13	-	-	-	3.83 ± 0.07	2.47 ± 0.02	2.81 ± 0.03	4.51 ± 0.21	5.39 ± 0.13	9.83 ± 0.11	1.39 ± 0.03	10.14 ± 0.09
Mrk 573	3.80 ± 0.18	4.04 ± 0.18	3.08 ± 0.17	14.05 ± 0.15	-	-	2.86 ± 0.01	3.92 ± 0.01	2.06 ± 0.01	2.76 ± 0.05	2.77 ± 0.04	1.48 ± 0.03	7.87 ± 0.43	-	4.26 ± 0.13
NGC 1144	4.72 ± 0.43	5.88 ± 0.35	4.28 ± 0.21	18.90 ± 0.21	2.14 ± 0.01	3.41 ± 0.01	3.30 ± 0.01	4.27 ± 0.04	2.31 ± 0.13	2.81 ± 0.01	4.01 ± 0.02	1.70 ± 0.09	10.63 ± 0.09	5.76 ± 0.01	-
Mrk 1066	4.05 ± 0.11	4.50 ± 0.08	3.61 ± 0.07	13.82 ± 0.14	-	1.90 ± 0.01	-	4.58 ± 0.01	2.25 ± 0.02	3.48 ± 0.13	3.68 ± 0.01	3.11 ± 0.02	9.98 ± 0.28	4.81 ± 0.13	7.87 ± 0.01
NGC 1275	-	-	-	-	-	-	-	-	-	2.71 ± 0.10	3.93 ± 0.08	2.49 ± 0.07	-	-	-
NGC 2110(‡)	5.28 ± 0.28	7.47 ± 0.90	4.59 ± 0.20	20.00 ± 0.20	-	2.28 ± 0.01	-	3.78 ± 0.05	1.81 ± 0.01	3.20 ± 0.28	3.30 ± 0.04	0.75 ± 0.01	4.78 ± 0.05	2.32 ± 0.10	4.20 ± 0.04
ESO 428-G014	4.31 ± 0.06	6.30 ± 0.04	3.85 ± 0.01	-	-	2.87 ± 0.07	-	4.77 ± 0.01	2.57 ± 0.01	3.40 ± 0.03	4.80 ± 0.06	2.31 ± 0.10	12.34 ± 0.34	5.10 ± 0.25	11.80 ± 0.11
Mrk 1210	-	-	-	-	-	-	-	6.54 ± 0.19	2.82 ± 0.16	3.35 ± 0.13	-	1.07 ± 0.16	7.73 ± 0.15	-	3.41 ± 0.47
NGC 5728	-	-	-	-	-	-	-	5.41 ± 0.17	3.74 ± 0.29	5.73 ± 0.12	8.74 ± 0.42	5.44 ± 0.14	8.16 ± 0.01	8.98 ± 0.01	10.27 ± 0.01
NGC 5929	3.56 ± 0.19	5.58 ± 0.17	4.06 ± 0.15	15.42 ± 0.25	-	1.00 ± 0.91	2.17 ± 0.91	4.27 ± 0.49	1.70 ± 0.19	3.52 ± 0.21	5.43 ± 0.17	3.67 ± 0.36	13.77 ± 0.06	6.78 ± 0.03	11.42 ± 0.04
NGC 5953(‡)	4.68 ± 0.23	6.50 ± 0.17	5.26 ± 0.13	12.65 ± 0.35	1.95 ± 0.01	1.98 ± 0.01	1.62 ± 0.01	3.98 ± 0.08	1.90 ± 0.04	3.61 ± 0.15	3.82 ± 0.03	2.67 ± 0.04	13.37 ± 0.20	7.74 ± 0.03	-
NGC 7674	2.24 ± 0.51	3.42 ± 0.43	3.57 ± 0.31	-	-	3.20 ± 0.36	-	2.35 ± 0.14	1.98 ± 0.03	-	-	-	-	-	-
NGC 7682	3.22 ± 0.20	4.53 ± 0.17	1.49 ± 0.30	11.00 ± 0.23	-	-	-	4.04 ± 0.08	2.92 ± 0.02	2.70 ± 0.02	-	-	9.42 ± 0.26	8.33 ± 0.08	-
Seyfert 1															
Mrk 334	-	-	-	19.11 ± 0.10	-	-	1.12 ± 0.11	3.40 ± 0.06	1.78 ± 0.08	3.13 ± 0.09	1.66 ± 0.04	1.85 ± 0.07	6.14 ± 0.01	2.96 ± 0.00	3.54 ± 0.05
NGC 1097	4.48 ± 0.17	5.84 ± 0.15	3.29 ± 0.13	5.88 ± 0.26	1.79 ± 0.22	1.46 ± 0.13	1.81 ± 0.13	4.51 ± 0.15	2.62 ± 0.20	3.69 ± 0.10	2.99 ± 0.01	2.04 ± 0.05	9.45 ± 0.20	5.16 ± 0.12	10.32 ± 0.02
MCG-5-13-17	2.35 ± 0.10	3.18 ± 0.08	3.84 ± 0.08	-	-	1.91 ± 0.21	-	2.87 ± 0.04	2.25 ± 0.05	3.07 ± 0.06	1.43 ± 0.05	1.97 ± 0.02	7.95 ± 0.11	3.87 ± 0.03	6.55 ± 0.05
Mrk 124	-	-	-	-	-	-	-	2.19 ± 0.06	1.29 ± 0.30	2.12 ± 0.05	-	-	-	-	-
NGC 3227	-	1.67 ± 0.06	2.09 ± 0.05	-	-	5.78 ± 0.15	-	3.43 ± 0.03	1.58 ± 0.03	-	2.36 ± 0.03	1.35 ± 0.04	6.24 ± 0.01	2.79 ± 0.00	4.47 ± 0.03
NGC 4051	-	-	-	-	-	-	-	3.22 ± 0.01	1.93 ± 0.03	3.19 ± 0.08	1.13 ± 0.01	0.73 ± 0.01	3.69 ± 0.11	0.66 ± 0.08	3.50 ± 0.02
Mrk 291	-	2.40 ± 0.07	4.45 ± 0.09	-	-	2.56 ± 0.01	-	3.43 ± 0.02	-	3.80 ± 0.11	-	-	11.90 ± 0.05	-	-
Arp 102B	-	-	-	-	-	-	-	2.12 ± 0.39	1.38 ± 0.07	3.82 ± 0.05	1.97 ± 0.03	2.14 ± 0.02	4.61 ± 0.05	2.80 ± 0.01	-
Mrk 896	-	-	-	-	-	-	-	1.69 ± 0.14	1.24 ± 0.25	2.16 ± 0.01	0.67 ± 0.08	0.53 ± 0.01	1.23 ± 0.06	1.89 ± 0.05	-

Notes. BP$_b$ and BP$_r$ are the blue and red bandpass boundaries. (‡) The continuum of W_{CaT} is affected by spurious emission. If we use only the points free from emission to set the continuum we get 3.28 ± 0.20, 5.03 ± 0.18 and 3.36 ± 0.17 for CaT$_1$, CaT$_2$, CaT$_3$, respectively.

Table 2. Continuum fluxes, normalized to unity at 1.223 μm.

Galaxy	$F\lambda/F_{1.223\mu m}$								
	0.81	0.88	0.99	1.06	1.22	1.52	1.70	2.09	2.19
(1)	(2)	(3)	(4)	(5)	(6)	(7)	(8)	(9)	(10)
					Seyfert 2				
NGC 262	1.28	1.12	1.11	1.01	1.00	0.94	0.95	0.95	0.92
Mrk 993	1.25	1.26	1.18	1.13	1.00	0.80	0.71	0.71	0.37
NGC 591	1.08	1.05	1.05	1.01	1.00	0.76	0.67	0.67	0.35
Mrk 573	1.26	1.27	1.23	1.15	1.00	0.79	0.72	0.72	0.45
NGC 1144	1.25	1.25	1.21	1.16	1.00	0.76	0.67	0.67	0.34
Mrk 1066	1.05	1.11	1.10	1.08	1.00	0.83	0.80	0.80	0.49
NGC 1275	1.47	1.29	1.20	1.16	1.00	0.87	0.81	0.73	0.73
NGC 2110	0.97	0.95	0.98	1.05	1.00	0.93	0.89	0.89	0.65
ESO 428-G014	1.18	1.17	1.12	1.08	1.00	0.79	0.72	0.72	0.37
Mrk 1210	-	1.25	1.27	1.16	1.00	0.85	0.82	0.82	0.65
NGC 5728	-	-	1.01	1.00	1.00	0.82	0.76	0.76	0.42
NGC 5929	1.25	1.24	1.15	1.10	1.00	0.80	0.73	0.73	0.35
NGC 5953	1.28	1.26	1.17	1.12	1.00	0.76	0.69	0.69	0.33
NGC 7674	1.21	1.12	1.08	1.02	1.00	0.97	1.02	1.02	1.10
NGC 7682	1.04	1.06	1.07	1.05	1.00	0.83	0.74	0.74	0.35
					Seyfert 1				
Mrk 334	1.07	1.07	1.08	1.06	1.00	0.93	0.91	0.91	0.69
NGC 1097	1.08	1.25	1.16	1.15	1.00	0.81	0.74	0.74	0.39
MCG-5-13-17	1.43	1.41	1.25	1.18	1.00	0.79	0.73	0.73	0.44
Mrk 124	-	-	1.00	1.00	1.00	1.07	1.06	1.06	1.00
NGC 3227	1.28	1.25	1.16	1.08	1.00	0.88	0.84	0.84	0.58
NGC 4051	-	1.27	1.15	1.07	1.00	0.89	0.86	0.86	0.73
Mrk 291	1.73	1.51	1.30	1.26	1.00	0.80	0.70	0.70	0.41
Arp 102B	1.48	1.33	1.24	1.23	1.00	0.77	0.69	0.69	0.40
Mrk 896	1.31	1.20	1.12	1.07	1.00	0.95	0.93	0.93	0.73

Note. The errors on F_λ are $\leq$3 per cent in all cases.

definitions.[3] Note that for NGC 3227, Terlevich et al. (1990) used an optional blue continuum band at λ 8582 Å, which provides a continuum slope very similar in both studies, which thus explains the similarity in $W_{\rm CaT}$.

In Fig. 1 we compare $W_{\rm Mg\,I}$ 1.58 μm with $W_{\rm Si\,I}$ 1.59 μm. These two absorption lines are correlated as $W_{\rm Si\,I} = (0.53 \pm 0.02) W_{\rm Mg\,I}$, with CC = 0.67 [or $W_{\rm Si\,I} = (0.71 \pm 0.21) W_{\rm Mg\,I}^{(0.8\pm0.2)}$, CC = 0.69]. The correlation between W_λ of these two lines suggests that almost all the objects studied here follow the same chemical enrichment. This hypothesis can be associated with the fact that Si and Mg are more abundant than the other α elements in the Galactic Globular Cluster NGC 6121, which is located near the Galaxy centre ($l = 350.^\circ97$, $b = 15.^\circ97$; Mariano et al. 2008).

We have tried diagrams involving other NIR absorption lines (or bands), but only weak correlations are found. Since the F_λ values are studied in Riffel et al. (2006) we only present them in Table 2 for comparison purposes.

Our sample is composed mostly of spiral galaxies (Table 3), which tend to increase the optical $W_{\rm Na\,I}$ with the inclination *b/a* (Bica et al. 1991). This could be the case of NGC 5728, which has a low *b/a*, high $W_{\rm Na\,I}$ and displays the highest $A_{\rm v} = 3.09$ mag value of our sample. In Fig. 2 we investigate the relation between galaxy inclination and W_λ of NIR absorption lines. The correlation

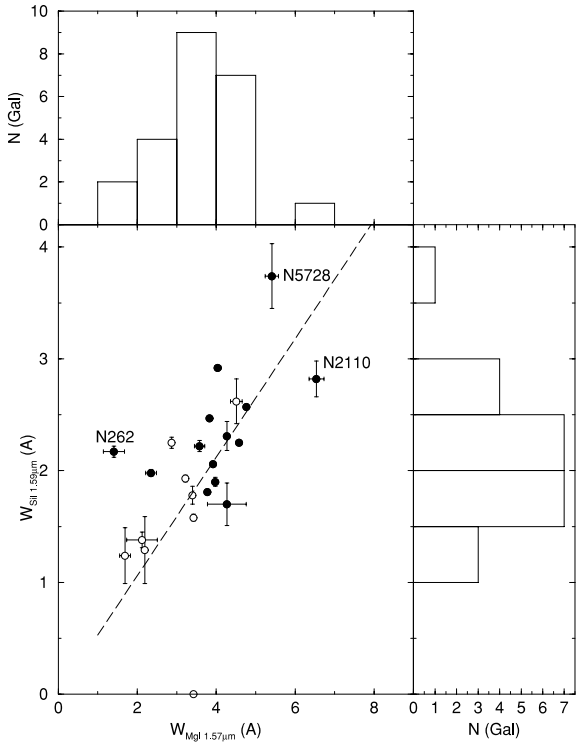

Figure 1. Diagram of $W_{\rm Mg\,I}$ 1.58 μm versus $W_{\rm Si\,I}$ 1.59 μm. The dashed line is the a liner correlation. Open symbols are Sy 1 and filled Sy 2.

[3] In order to compare our $W_{\rm CaT}$ values with those of Terlevich et al. (1990) we compute the $W_{\rm CaT}$ of our NGC 5953 spectrum using their continuum definition. The values thus obtained are $W_{\rm CaT1} = 1.7$ Å, $W_{\rm CaT2} = 4.3$ Å, and $W_{\rm CaT3} = 3.8$ Å, which are very similar to those of Terlevich et al. (1990).

Table 3. Synthesis results. For more details, see text.

Galaxy	$b/a^{\dagger}$	Morphology‡	FC (per cent)	BB_c (per cent)	BB_h (per cent)	x_Y (per cent)	x_I (per cent)	x_O (per cent)	m_Y (per cent)	m_I (per cent)	m_O (per cent)	χ^2	adev	Av (mag)	$\langle \log t_\star \rangle_L$ (yr)	$\langle \log t_\star \rangle_M$ (yr)	$\langle Z_\star \rangle_L$ (*)	$\langle Z_\star \rangle_M$ (*)
(1)	(2)	(3)	(4)	(5)	(6)	(7)	(8)	(9)	(10)	(11)	(12)	(13)	(14)	(15)	(16)	(17)	(18)	(19)
								Seyfert 2										
NGC 262	1.0	S0-a	20.0	1.8	3.6	0.0	13.0	61.2	0.0	2.9	97.1	1.52	1.06	1.37	9.68	9.89	0.011	0.005
Mrk 993	0.32	Sa	4.7	0.0	0.0	0.0	27.8	66.8	0.0	6.4	93.6	0.01	1.90	1.32	9.54	9.83	0.013	0.005
NGC 591	0.77	S0-a	0.0	0.0	0.0	14.9	27.4	57.5	1.4	7.5	91.1	0.01	2.87	1.97	9.28	9.84	0.014	0.003
Mrk 573	1.0	S0-a	22.4	0.0	0.0	11.9	52.6	11.8	3.4	45.1	51.5	2.98	1.02	0.99	8.93	9.56	0.028	0.024
NGC 1144	0.64	E	0.0	0.0	0.0	0.0	71.3	26.1	0.0	44.9	55.1	0.01	2.22	1.44	8.97	9.32	0.021	0.015
Mrk 1066	0.59	S0-a	17.9	0.0	0.0	4.6	50.7	26.8	0.8	29.8	69.5	2.36	1.11	1.54	9.19	9.67	0.025	0.015
NGC 1275	0.77	S0	65.8	0.3	0.0	2.8	0.0	32.1	0.1	0.0	99.9	1.15	0.80	0.22	9.68	9.94	0.003	0.001
NGC 2110	0.76	E-SO	33.6	0.0	0.9	9.5	36.3	18.9	1.7	26.0	72.3	1.42	0.75	1.98	8.98	9.70	0.028	0.010
ESO 428-G014	0.58	S0	0.0	0.0	0.0	9.2	49.1	39.6	1.1	15.9	83.0	0.03	2.05	1.52	9.13	9.76	0.021	0.005
Mrk 1210	1.0	S?	12.0	0.5	0.0	9.2	48.8	29.1	0.3	30.7	69.0	2.29	1.05	1.14	9.17	9.77	0.013	0.007
NGC 5728	0.58	Sa	0.0	0.0	0.0	0.0	69.5	27.8	0.0	24.4	75.6	0.01	2.89	3.09	8.64	9.51	0.037	0.037
NGC 5929	0.78	Sa	0.0	0.0	0.0	7.3	24.5	69.7	1.4	11.0	87.7	0.01	2.38	1.48	9.37	9.61	0.020	0.022
NGC 5953	0.81	S0-a	0.0	0.0	0.0	0.0	33.5	65.2	0.0	7.0	93.0	0.01	2.00	0.81	9.46	9.80	0.031	0.023
NGC 7674	0.91	SBbc	29.2	2.2	5.7	3.4	24.6	35.6	0.7	15.8	83.4	0.03	1.37	1.03	9.28	9.69	0.018	0.010
NGC 7682	0.92	Sab	0.0	0.0	0.0	0.0	34.7	62.2	0.0	6.4	93.6	0.02	3.76	1.89	9.53	9.91	0.020	0.011
								Seyfert 1										
Mrk 334	0.70	Sbc	23.7	0.0	8.2	12.2	24.1	31.7	2.6	9.9	87.5	0.01	1.45	1.36	9.03	9.71	0.018	0.007
NGC 1097	0.67	SBb	4.3	0.0	0.0	19.8	46.4	29.8	2.9	28.6	68.5	1.70	1.33	1.29	8.88	9.49	0.024	0.017
MCG-5-13-17	0.67	E-SO	6.6	0.0	3.9	22.9	45.7	21.6	5.2	25.1	69.7	1.68	0.81	0.88	8.55	9.47	0.023	0.012
Mrk 124	0.67	S?	36.5	0.0	22.6	3.6	18.3	19.0	1.4	14.8	83.8	0.10	1.29	0.81	9.10	9.73	0.008	0.002
NGC 3227	0.66	SABa	31.0	0.0	2.1	38.4	28.1	0.0	10.8	89.2	0.0	0.05	1.24	0.99	8.00	9.07	0.011	0.011
NGC 4051	0.75	SABb	41.0	0.0	6.8	37.6	14.4	0.0	46.7	53.1	0.2	0.03	1.28	0.57	7.53	8.02	0.020	0.010
Mrk 291	0.67	SBa	6.5	0.0	4.5	0.0	6.1	85.3	0.0	1.1	98.9	1.01	2.06	0.45	9.85	9.94	0.006	0.004
Arp 102 B	0.78	?	7.9	0.0	3.0	11.7	35.2	41.5	1.0	12.7	86.3	1.61	1.14	0.68	9.08	9.80	0.015	0.005
Mrk 896	0.72	Sab	27.0	0.0	13.7	4.5	2.3	53.0	0.5	0.6	98.9	0.01	0.90	0.55	9.72	9.96	0.009	0.012

†From NED.

‡From HyperLeda – Data base for physics of galaxies (http://leda.univ-lyon1.fr; Paturel et al. 2003).

*Abundance by mass with $Z_{\odot} = 0.02$.

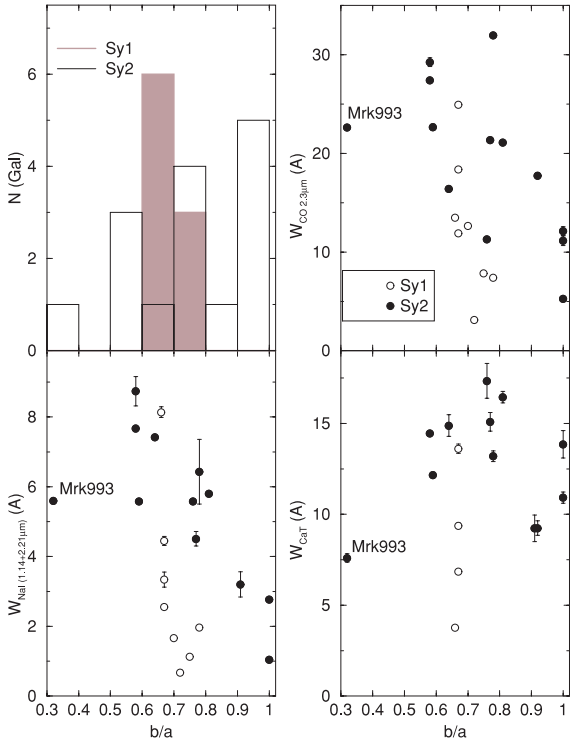

Figure 2. Diagrams of W_λ versus *b/a*. At top left the *b/a* histogram of our galaxies. The other three plots show *b/a* versus $W_{CO\,2.3\,\mu m}$, W_{NaI} and W_{CaT}, respectively. Open symbols are Sy 1 and filled Sy 2.

suggests that the interstellar medium plays an important role in the NIR W_{NaI}.[4] On the other hand, W_{CO} is weakly correlated with galaxy inclination (Fig. 2, top right), suggesting a weaker dependence on the interstellar medium. No correlation of W_{CaT} with *b/a* is found. In addition, the correlation between NaI and W_{CO} 2.3 μm with *b/a* has no evident relation with Seyfert type (Fig. 2).

4 SPECTRAL SYNTHESIS

In this section we study the NIR SP of our galaxy sample, fitting the underlying continuum of the 24 AGNs in the spectral range between 0.8 and 2.4 μm.

4.1 The base set

Clearly, the most important ingredient in the SP synthesis is the spectral base set, $b_{j,\lambda}$. An ideal base of elements should cover the range of spectral properties observed in the galaxy sample, providing enough resolution in age and metallicity to properly address the desired scientific question (Schmidt et al. 1991, CF05).

One improvement here over previous approaches that attempted to describe the stellar content of active galaxies using NIR spectroscopy is the inclusion of EPS models that take into account the effects of TP-AGB stars. Accordingly, we use as base set the EPS of Maraston (2005). The SSPs used in this work cover 12 ages, $t = 0.01$, 0.03, 0.05, 0.1, 0.2, 0.5, 0.7, 1, 2, 5, 9, 13 Gyr, and four metallicities, namely $Z = 0.02\,Z_\odot$, $0.5\,Z_\odot$, $1\,Z_\odot$ and $2\,Z_\odot$, summing up 48 SSPs.

[4] The better NIR correlation can also be associated with the fact that the NIR probes SPs deeper in the dust and therefore the contribution of the NaI is enhanced by the intrinsic stellar light.

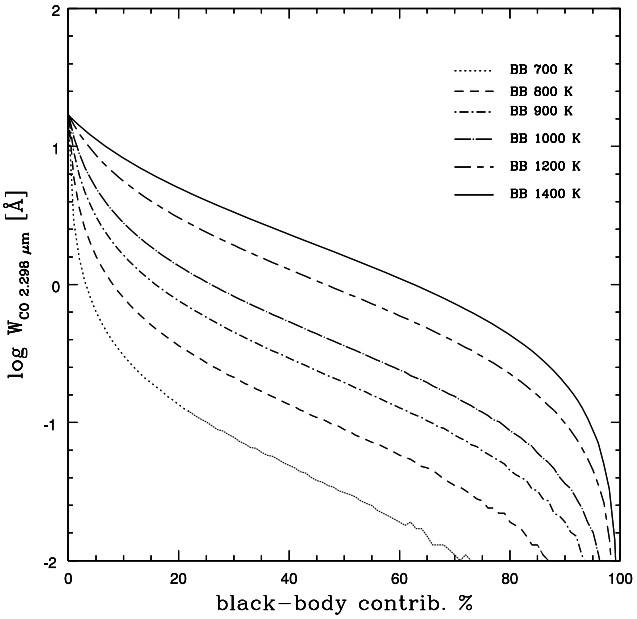

Figure 3. Effect on W_{CO} of the combination of the template derived for the starburst galaxy NGC 7714 with blackbody distributions at different temperatures. We use increasing BB fractions from 1 per cent to 100 per cent. BB temperatures are labelled.

When trying to describe the continuum observed in AGNs, the signature of the central engine cannot be ignored. Usually, this component is represented by a featureless continuum (FC; e.g. Koski 1978, CF04) of power-law form that follows the expression $F_\nu \propto \nu^{-1.5}$. Therefore, this component was also added to the base of elements. The contribution of this continuum (in percentage) to the flux at λ_0 (1.223 μm) is denoted by FC in Table 3. According to the unified model (e.g. Antonucci & Miller 1985; Antonucci 1993), the FC in Sy 2 galaxies (if present) is due to scattered light from the hidden Seyfert 1 (Sy 1) nucleus. However, the reader must bear in mind that a common problem in the study of the SP of Seyfert galaxies (especially in the optical) is that a reddened young starburst ($t \leq 5$ Myr) is indistinguishable from an AGN-type continuum (see Section 5.2; Cid Fernandes & Terlevich 1995; Storchi-Bergmann et al. 2000, CF04). To avoid this problem we have not included very young SSPs in our base (this point is also discussed in Section 5.2).

In the spectral region studied here, hot dust plays an important role in the continuum emission of active galaxies. Previous studies (i.e. Riffel et al. 2006, for instance) report a minimum in the continuum emission around 1.2 μm, probably associated with the red end of the optical continuum related to the central engine and the onset of the emission due to reprocessed nuclear radiation by dust (Barvainis 1987; Thompson 1995; Rudy et al. 2000; Rodríguez-Ardila & Viegas 2003; Rodríguez-Ardila & Mazzalay 2006; Riffel et al. 2006). In order to properly account for this component, we have included in our spectral base eight Planck distributions (blackbody – BB), with T ranging from 700 to 1400 K, in steps of 100 K. The lower limit in T is due to the fact that lower temperatures are hard to detect. Even a small fractional contribution would require a sizeable amount of dust. In order to illustrate this point, we plot in Fig. 3 combinations of different BB distributions with the synthetic template of the starburst galaxy NGC 7714, derived by Riffel et al. (2008b).The combination was made by summing up, in the whole spectral range, increasing fractions of the dust component from 0 to 100 per cent. Thus, we start with the pure NGC 7714 synthetic

spectrum and end with a pure BB distribution according to

$$F = \left(1 - \frac{f}{100}\right) F_{\rm SP} + \left(\frac{f}{100}\right) F_{\rm BB}, \quad (1)$$

where f is the percentual flux, which we vary in steps of 1 per cent, $F_{\rm SP}$ is the flux of the synthetic spectrum of NGC 7714 normalized to unity at 1.223 μm and $F_{\rm BB}$ is the BB flux also normalized at the same wavelength. As can be observed in Fig. 3, small fractional contributions of cool (<700 K) dust can significantly alter the strength of the absorption lines of the K-band spectrum, and therefore, are very hard to be detected in our spectral range. Hotter BB distributions are not used because 1400 K is very close to the sublimation temperature of graphite grains (likely the main constituent of the dust; Barvainis 1987; Rodríguez-Ardila & Mazzalay 2006).

4.2 The method

The second most important ingredient of an SP synthesis is the code that will suitably combine the individual components of the base elements to construct the final model that will represent the observed continuum. Here, as a synthesis code, we use for the first time – in this spectral range – the STARLIGHT software (CF04; Cid Fernandes et al. 2005a, hereafter CF05; Mateus et al. 2006; Asari et al. 2007; Cid Fernandes et al. 2009). This code is well described in CF04 and CF05. In summary, STARLIGHT mixes computational techniques originally developed for semi-empirical population synthesis with ingredients from evolutionary synthesis models (CF05). Basically, the code fits an observed spectrum O_λ with a combination, in different proportions, of $N_\star$ single stellar populations (SSPs). Due to the fact that the Maraston (2005) models include the effect of the TP-AGB phase, crucial to model NIR SP (see Riffel et al. 2007, 2008b), we used this EPS models as the base set for STARLIGHT.[5] Extinction is modelled by STARLIGHT as due to foreground dust, and parametrized by the V-band extinction A_V. We use the CCM (Cardelli, Clayton & Mathis 1989) extinction law. Essentially, the code solves the following equation for a model spectrum M_λ (CF05):

$$M_\lambda = M_{\lambda 0} \left[\sum_{j=1}^{N_\star} x_j\, b_{j,\lambda}\, r_\lambda\right] \otimes G(v_\star, \sigma_\star), \quad (2)$$

where $b_{j,\lambda}\, r_\lambda$ is the reddened spectrum of the jth SSP normalized at λ_0; $r_\lambda = 10^{-0.4(A_\lambda - A_{\lambda 0})}$ is the reddening term; $M_{\lambda 0}$ is the synthetic flux at the normalization wavelength; $\boldsymbol{x}$ is the population vector; $\otimes$ denotes the convolution operator and $G(v_\star, \sigma_\star)$ is the Gaussian distribution used to model the line-of-sight stellar motions; it is centred at velocity $v_\star$ with dispersion $\sigma_\star$.

The fit is carried out with a simulated annealing plus Metropolis scheme, which searches for the minimum of the equation (CF05):

$$\chi^2 = \sum_\lambda [(O_\lambda - M_\lambda) w_\lambda]^2 \quad (3)$$

where emission lines and spurious features are masked out by fixing $w_\lambda = 0$. For more details on STARLIGHT, see CF04 and CF05.

5 SYNTHESIS RESULTS AND DISCUSSION

We present in Figs 4–9 the results of the spectral synthesis fitting procedure. For each galaxy the top panel shows the observed and synthetic spectra normalized to unity at 1.223 μm. Note that in all cases the synthetic spectrum was shifted by a constant for visualization purposes. The bottom panel shows the residual spectrum $O_\lambda - M_\lambda$. As expected, the residual is dominated by the nebular emission. The analysis of the emission lines free from the SP contamination is beyond the scope of this paper and is left for a forthcoming work (Riffel et al., in preparation). The results of the synthesis are summarized in Table 3. The quality of the fits is measured by the χ^2 (Column 13)[6] and the *adev* (Column 14) parameters. The latter gives the percentage mean deviation $|O_\lambda - M_\lambda|/O_\lambda$ over all fitted pixels.

To take into account noise effects that dump small differences between similar spectral components, we followed CF05 and present our results using a condensed population vector, which is obtained by binning the $\boldsymbol{x}$ into young, $x_{\rm Y}$ ($t_j \leq 5 \times 10^7$ yr), intermediate-age, $x_{\rm I}$ ($1 \times 10^8 \leq t_j \leq 2 \times 10^9$ yr) and old, $x_{\rm O}$ ($t_j > 2 \times 10^9$ yr) components, using the flux contributions. The same bins were used to represent the mass components of the population vector: $m_{\rm Y}$, $m_{\rm I}$ and $m_{\rm O}$, respectively. The condensed population vectors are presented in Columns 7–12 of Table 3. For more details on vector definition, see CF05. We have also binned the blackbody contributions into two components. The cool ($BB_{\rm c}$) is obtained by summing up the BB contributions with $T \leq 1000$ K, and the hot one ($BB_{\rm h}$) with $T \geq 1100$ K. These components were defined based on the sublimation temperatures of silicate (∼1000 K) and graphite (∼1200 K) grains (Barvainis 1987; Granato & Danese 1994). The condensed blackbody vectors for each source are listed in Columns 5 and 6 of Table 3.

The spectral synthesis shows that the NIR continuum of active galaxies can be explained in terms of at least three components: a non-thermal continuum, the dust emission and the SP of the circumnuclear region. As can be seen in Table 3 and in Fig. 10, the contribution of the latter to the nuclear continuum is higher than 50 per cent in most objects. Therefore, its study is a critical step in the analysis of the continuum emission of Seyfert galaxies. Moreover, our results are consistent with the predictions of the unified model for AGNs, as the non-thermal continuum and the hot dust emission are present in all Sy 1 sources and only in a small fraction of the Sy 2s (see also Section 5.3). In the following sections we provide a detailed description of each of these three components in the light of the results obtained here and compare them with those obtained in other wavelength regions, mostly in the optical.

5.1 The stellar population

Binning the population vectors into six components[7] left us with a coarser but more powerful description of the SFH of our galaxy sample. To better quantify the NIR SFH we plot a histogram with the flux-weighted and mass-weighted condensed population vectors in Fig. 11. Overall, the NIR SPs are heterogeneous, as in most sources the three components contribute significantly to the integrated flux. However, the contribution of $x_{\rm Y}$ is very small ($\lesssim$10 per cent) for most of our sample. The intermediate-age component is well distributed, with a maximum centred at ∼40 per cent. The $x_{\rm O}$ contribution is very similar to that of the intermediate age.

Regarding the mass-weighted components, as expected from the results seen above, the contribution of $m_{\rm Y}$ is very small (near zero) as

[5] As a default base set, the code uses the SSPs of Bruzual & Charlot (2003).

[6] This, in fact, is the χ^2 divided by the number of λs used in the fit. Reliable fits are obtained when $\chi^2 \sim 1$ (CF04). For more details see STARLIGHT, manual available at http://www.starlight.ufsc.br.

[7] With three components representing the star formation episodes.

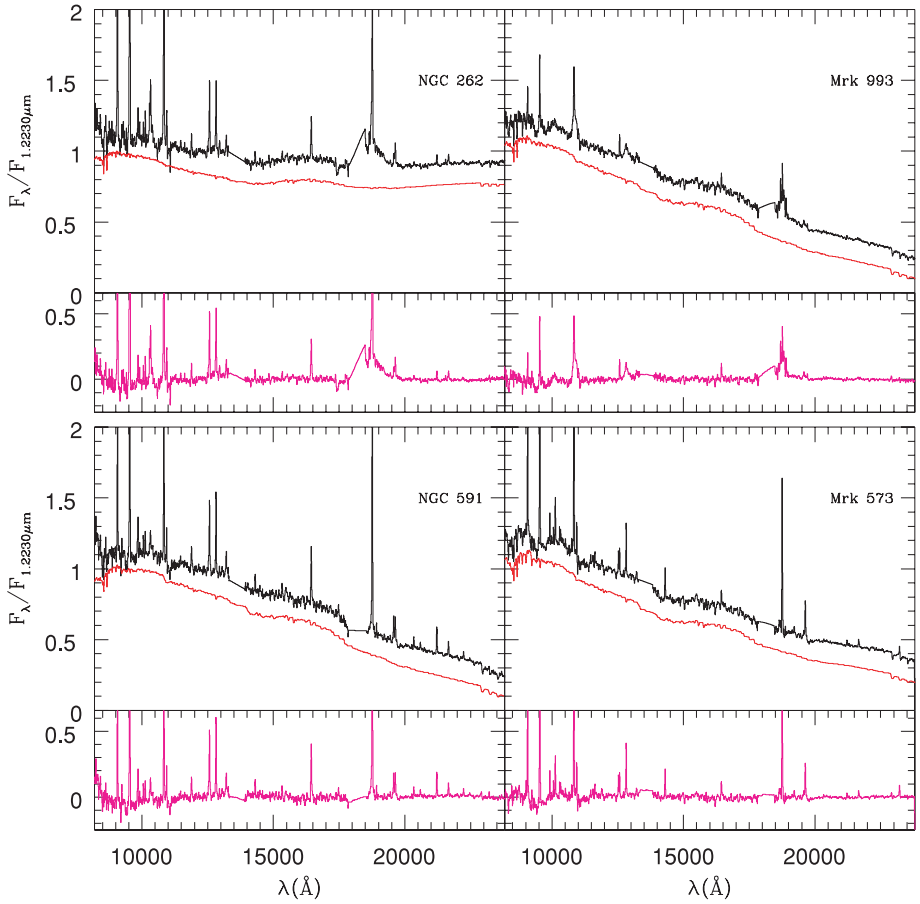

Figure 4. Spectral fits. Each panel shows (i) at top the flux of the observed spectrum, normalized at unity at 1.223 μm, and the synthetic spectra (shifted down for clarity); (ii) at bottom the $O_\lambda - M_\lambda$ residual spectrum.

can be observed in the right-hand side of Fig. 11. The intermediate-age mass contributions are distributed over all fractions (from 0 to 100 per cent) but tend to be biased to values lower than 20 per cent. In contrast, the old component of the mass-weighted vector is biased to values higher than 70 per cent.

According to CF05, if one would characterize the SP mixture of a galaxy by a single parameter, it is the mean stellar age. They defined it in two ways: the first is weighted by light fraction,

$$\langle \log t_\star \rangle_{\rm L} = \sum_{j=1}^{N_\star} x_j \log t_j, \quad (4)$$

and the second, weighted by the stellar mass,

$$\langle \log t_\star \rangle_{M} = \sum_{j=1}^{N_\star} m_j \log t_j. \quad (5)$$

Note that both definitions are limited by the age range used in our elements base (Section 4.1) and obviously, the FC and BB components were excluded from the sum. The mean stellar ages derived with both definitions are presented in Columns 16 and 17 of Table 3, respectively.

To better quantify the NIR mean ages we show at the left-hand side of Fig. 12 histograms for $\langle \log\, t_\star \rangle_{\rm L}$ and $\langle \log\, t_\star \rangle_{M}$. The light-weighted mean age of our galaxy sample is biased to an intermediate/old age SP, while for the mass-weighted mean age we clearly observe that the old population dominates. As stated by CF05 the mass-weighted mean age is a more physical parameter, but it has a much less direct relation with the observables. They associated this discrepancy with the non-constant stellar M/L ratio.

A secondary parameter to describe the mixed SP is the metallicity. CF05 also defined the light-weighted mean metallicity by

$$\langle Z_\star \rangle_{\rm L} = \sum_{j=1}^{N_\star} x_j Z_j, \quad (6)$$

as well as the mass-weighted mean metallicity, which is represented by

$$\langle Z_\star \rangle_{M} = \sum_{j=1}^{N_\star} m_j Z_j. \quad (7)$$

Both definitions are bounded by the $\frac{1}{50}\,Z_\odot$–$2\,Z_\odot$ range. The light- and mass-weighted mean metallicities, estimated for our galaxies, are presented in Columns 18 and 19 of Table 3, respectively.

We present in the right-hand side of Fig. 12 a histogram for the light- and mass-weighted metallicities of our sample. Our results point to a mean metallicity solar to above solar, if we consider the light-weighted values, while for the mass-weighted mean metallicity our results indicate a subsolar value. We associate this discrepancy with the well-known age–metallicity degeneracy, i.e. for a fixed mass, a high-metallicity SP looks cooler – and older – than a low-metallicity SP, thus resulting in a higher M/L ratio. Moreover, this is consistent with a galaxy chemical enrichment scenario in which the young population is enriched by the evolution of the early massive stars. In this context, the light-weighted metallicity is

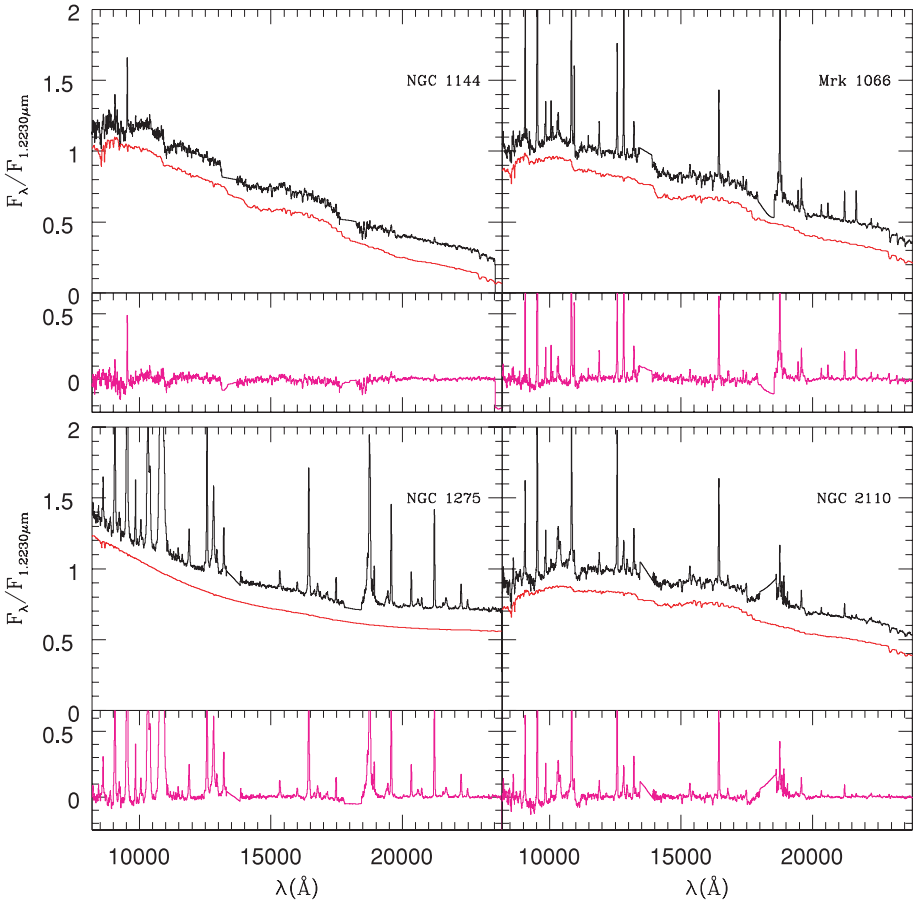

Figure 5. Same as Fig. 4.

more sensitive to the young component, while the mass-weighted metallicity is more sensitive to the old SP.

5.1.1 *Previous studies*

A significant fraction (12 out of 24) of our objects have been the subject of previous SP studies in the optical and UV regions. In this section we will compare our NIR results with those available in the literature.

(i) *NGC 262.* According to Garcia-Vargas et al. (1989), most of the optical and NIR flux comes from the galaxy bulge SP. The emission at shorter wavelengths can be fitted by a power law. González Delgado, Heckman & Leitherer (2001) studied the optical SP of this galaxy and found a dominant old population. By fitting the nuclear continuum with an off-nuclear spectrum of the galaxy bulge as template, they conclude that the contribution of a power law is unnecessary. In the case of an elliptical as a template spectrum, they needed to include a contribution ≤25 per cent of a power law ($F_\lambda \propto \lambda^{-1}$). They argue that such a small dilution can be related to a change in the SP of NGC 262 with respect to the elliptical galaxy template. Similar results are obtained by Raimann et al. (2003). They found 60 per cent, 20 per cent, 12 per cent and 8 per cent for the old, intermediate, young and FC components, respectively.[8]

[8] Note that we have used only the nuclear region. We use the 10 Gyr, 1 Gyr, 100+10 Myr and 3 Myr+FC as old, intermediate, young and FC components, respectively.

As can be observed in Table 3, our results agree with the optical studies.

(ii) *ESO 428−G014.* CF04 carried out a study of the SP in the spectral region between 3500 and 5200 Å of the inner 200 pc of this source. Their study also used STARLIGHT. They found x_Y = 20 per cent, x_I = 47 per cent and x_O = 33 per cent. As can be observed in Table 3, our NIR results agree with those obtained by CF04 in the optical.

(iii) *Mrk 1066.* The light in the optical region of this galaxy is dominated by young- to intermediate-age SPs, and the nuclear spectrum is strongly diluted by a non-thermal component (González Delgado et al. 2001). These results agree with those reported by Raimann et al. (2003). Our results show that light at 1.22 μm is dominated by an intermediate-age SP diluted by an FC component, in agreement with the optical results (see Table 3). With respect to the stellar component, our results agree with Ramos Almeida, Pérez García & Acosta-Pulido (2009), which studied the same spectral region by modelling the continuum with combinations of stars and black-body (with T = 1000 K) dilution, without the FC component.

(iv) *Mrk 1210.* The optical SP of this source has been studied by many authors (Schmitt, Storchi-Bergmann & Cid Fernandes 1999; Storchi-Bergmann et al. 2000, CF04); however, the results are controversial. While Schmitt et al. (1999) argue that the optical light is dominated by a 10 Gyr population (54 per cent at λ 5870 Å), Storchi-Bergmann et al. (2000) suggest that a young SP (or a power law) contributes with 50 per cent of the flux observed in λ4020 Å. When modelling the spectral interval between λ3500 and λ5200 Å, CF04 inferred that 53 per cent of the flux observed in the spectrum

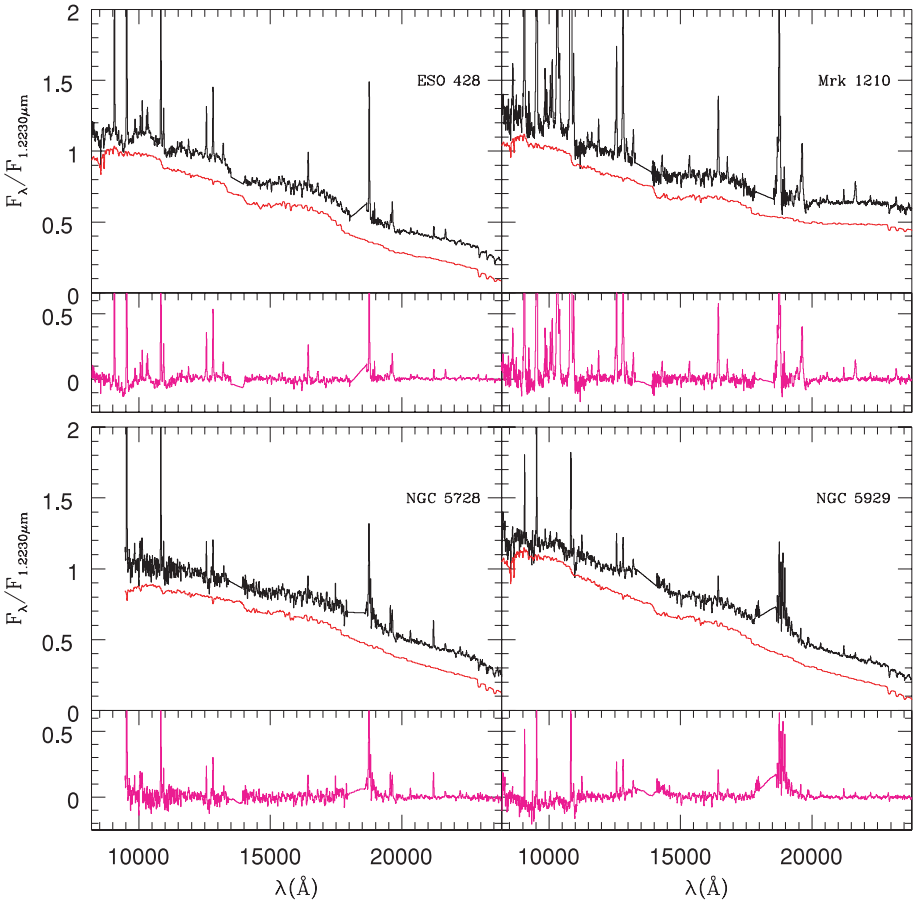

Figure 6. Same as Fig. 4.

Mrk 1210 was due to a young SP. They also found a contribution of 39 per cent for the old component and 5 per cent for the intermediate one. Our results disagree with those reported in the optical, as we found a lower fraction for the old component (∼29 per cent) and ∼49 per cent for the intermediate one. Moreover, ∼20 per cent of the flux belongs to young+FC components.

(v) *NGC 3227.* We found a dominant young component (∼40 per cent) for this galaxy. Our results agree with those of Davies et al. (2006, 2007) which analyse the star formation in the inner 10 pc of this galaxy using the near infrared adaptive optics integral field spectrograph SINFONI. They found that the light in this region is dominated by a 40 Myr SP.

(vi) *Mrk 573.* The optical SP of this source was studied by Schmitt et al. (1999). They fit the W_λ and continuum ratios, finding that 82 per cent of the flux observed in λ 5870 Å is due to a 10 Gyr SP. These results are in good agreement with those obtained by Raimann et al. (2003), Storchi-Bergmann et al. (2000) and González Delgado et al. (2001) in the optical region.[9] Our NIR spectral synthesis points to a dominant intermediate-age population (∼53 per cent) diluted by an FC component, which contributes with ∼22 per cent of the observed continuum flux. As for Mrk 1066, we agree with Ramos Almeida et al. (2009) with respect to the dominant presence of an intermediate age population, but we only found dilution by the FC component.

(vii) *NGC 1097.* The SP of this galaxy was studied in the UV by Bonatto et al. (1998). They infer that the light at λ2646 Å is due to a fraction of ∼40 per cent of a young SP,[10] 16 per cent to intermediate-age and ∼44 per cent to old SP. These results agree with the detection of a young starburst in the inner 9 pc of this galaxy (Storchi-Bergmann et al. 2005; see also Davies et al. 2007, 2009) and with the optical SP studied by CF04, who found a contribution of 31 per cent for the young component. However, there are some differences between the UV and optical SP for the intermediate-age (CF found 37 per cent) and for the old (CF found 12 per cent, they also determine 19 per cent for the FC) components. The results for the young SP of both groups of authors are consistent with our NIR synthesis. Regarding the intermediate- and old-age components, our results are more consistent with those of the optical region. The discrepancies between our results and those obtained in the UV are probably related to the fact that in the NIR we are integrating light through a deeper line of sight and, thus, we detect old stars located more internally in the bulge of the galaxy.

(viii) *NGC 2110.* González Delgado et al. (2001) argue that the stellar optical absorption lines are similar to those of an old population. By fitting the nuclear continuum with an off-nuclear spectrum of the galaxy bulge as template, they conclude that the contribution of a power law is unnecessary. In the case of an elliptical as a template spectrum, they needed to include a contribution ≤25 per cent

[9] These two latter groups have analysed the absorption line species present in the observed spectra.

[10] We call young SP the sum of the contributions with age ≤0.2 Gyr. For more details, see table 11 of Bonatto et al. (1998).

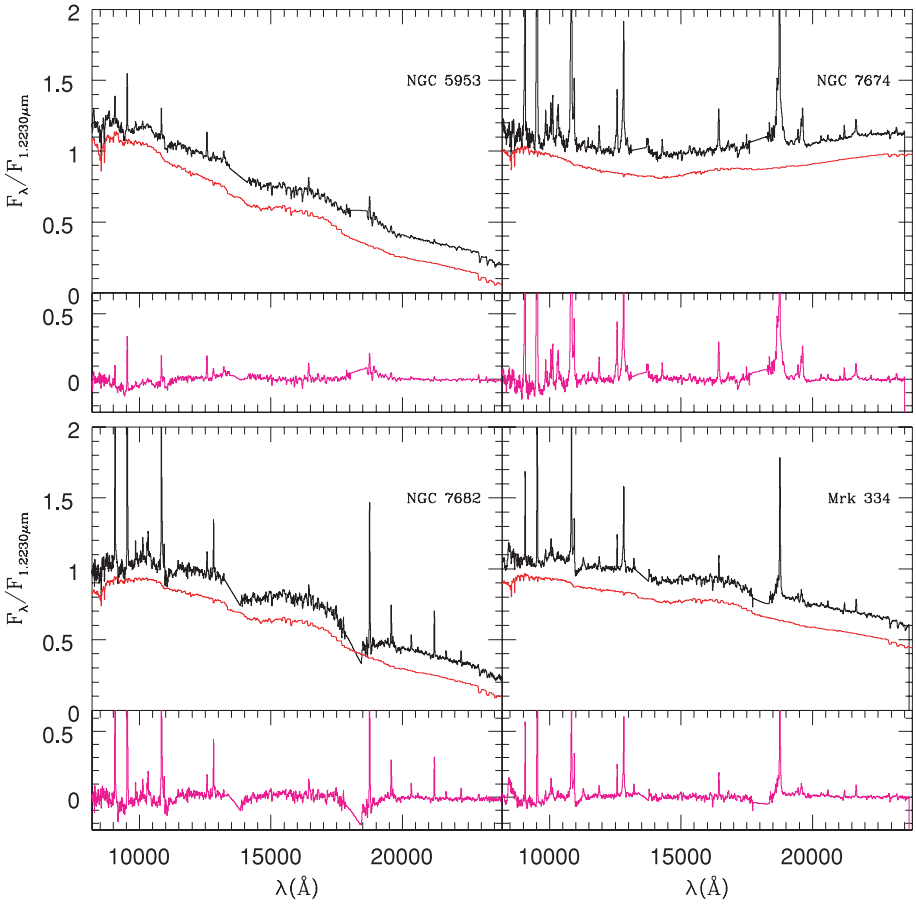

Figure 7. Same as Fig. 4.

of a power law ($F_\lambda \propto \lambda^{-1}$). These results are further confirmed by CF04, who found a contribution of 67 per cent for the old component, 7 per cent for the intermediate-age and 26 per cent for the young SP, as well as by Raimann et al. (2003) who determine contributions of 53 per cent, 32 per cent and 10 per cent for the old-, intermediate- and young-age components, respectively. Our results indicate a dominant intermediate-age SP and a strong FC component. The detection of the latter component may be related to the fact that the NIR is less affected by dust extinction and is consistent with the detection of broad components in the emission lines (see Section 5.2).

(ix) *NGC 5728.* CF04 fitted the SP of this object and concluded that its light between 3500 and 5200 Å is dominated by intermediate-age stars (51 per cent), with contributions of 20 per cent and 28 per cent of young and old SPs, respectively. These fractions agree with our NIR analysis, where we found a dominant contribution of the intermediate-age SP (∼70 per cent) and ∼30 per cent for the old component. However, we did not detect the young component in our fitting process. This can be associated with the fact that NIR light is dominated by intermediate-age stars (Maraston 2005) or to our spectral coverage that misses the calcium triplet absorption, lines which are more sensitive to young SPs (see fig. 4 of Riffel et al. 2008b).

(x) *NGC 5929.* According to González Delgado et al. (2001), the nucleus of this source is dominated by an old SP, a conclusion obtained by studying the W_λ of optical absorption lines. They also conclude that if the off-nuclear spectrum is used as a template to fit the nuclear spectrum of NGC 5929, no signs of dilution are observed. Similar results are obtained by Raimann et al. (2003), who found contributions of 61 per cent, 27 per cent, 8 per cent and 4 per cent for the old, intermediate and young and FC components, respectively. These results fully match our NIR synthesis (FC = 0 per cent, $x_Y = 7.7$ per cent, $x_I = 24.5$ per cent and $x_O = 69.7$ per cent).

(xi) *NGC 5953.* One of the galaxies studied by CF04. They derived a dominant intermediate-age optical SP ($x_I = 74$ per cent) with small fractions of young and old stars ($x_Y = 1$ per cent and $x_O = 7$ per cent) and a contribution of 18 per cent of the FC. The NIR SP of this galaxy is divided into two components, the old, dominant, (∼65 per cent) and the intermediate age (∼34 per cent). The FC component does not contribute to the NIR flux.

(xii) *NGC 7682.* The optical light of this source is dominated by an old SP (86 per cent) with no contribution of intermediate-age stars (CF04). A small contribution of young populations (8 per cent) and 6 per cent of an FC component is reported by CF04. Our NIR results disagree with those of the optical: the SP is shared between old (∼63 per cent) and intermediate (∼35 per cent) age populations.

Our NIR synthesis and that in the optical (CF04) have been analysed by the same method (the STARLIGHT code), allowing for a proper comparison of the objects in common to both studies. Fig. 13 summarizes this comparison. In general, our results do not agree with those in the optical. Part of the differences can be accounted for by the fact that the NIR is more suitable for the identification of old SPs and the detection of the unique absorptions related to

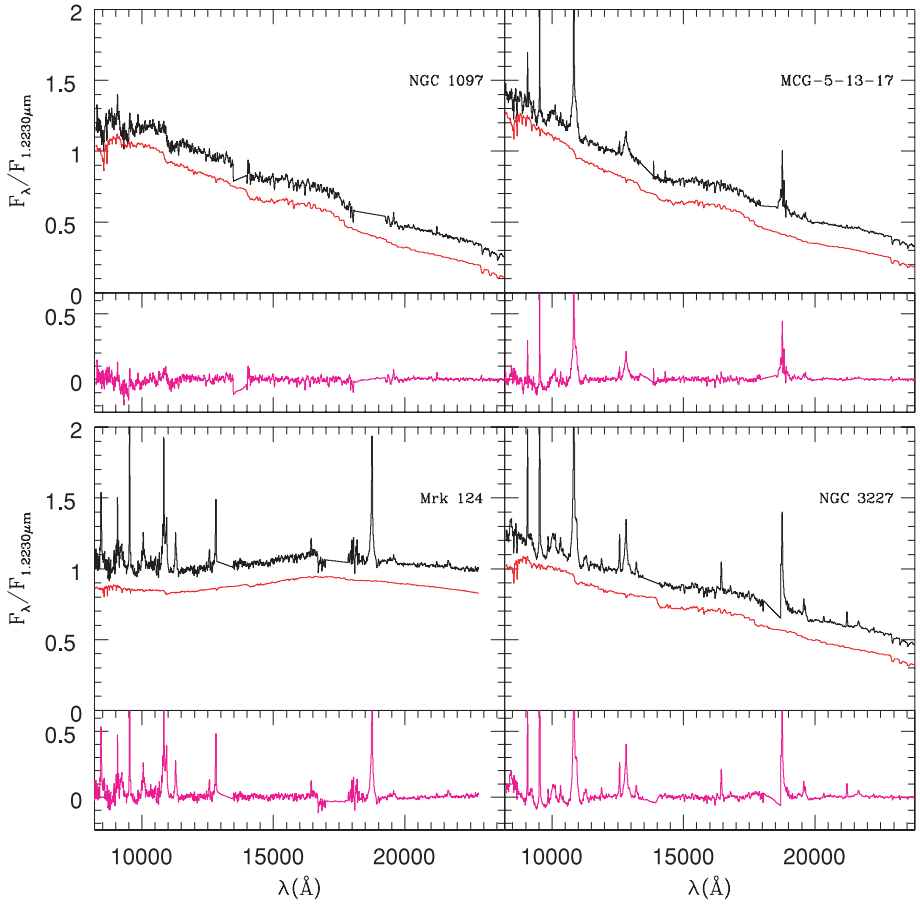

Figure 8. Same as Fig. 4.

1-Gyr-old SP featured by TP-AGB stars (Riffel et al. 2008b). This hypothesis is appropriate for the case of NGC 5953, where the differences between our results and those of CF04 occur in the x_I and x_O components. In addition, the differences between optical and NIR SPs can be associated with the fact that the NIR probes SPs buried deep in the dust. An example of this situation is NGC 2110, where we have detected the presence of hot dust in its integrated spectrum (Table 4). For the case of NGC 1097, Storchi-Bergmann et al. (2005) report an obscuration of a central starburst, which they associate with a dusty absorbing medium.

Our finding that the central regions of the galaxies contain a substantial fraction of intermediate-age SPs (see Figs 11 and 14), together with the prolonged SFH, is very similar to the picture drawn in the case of central star-forming rings, based on optical data (Allard et al. 2006; Sarzi et al. 2007). This might support the scenario where central star formation often occurs in circumnuclear rings (Sarzi et al. 2005; Shields et al. 2007).

5.1.2 The CN versus intermediate-age stellar population

Our NIR approach offers a unique opportunity to investigate in a more consistent way the relation between the CN molecular band and the unambiguous evidence of an intermediate-age SP (Maraston 2005; Riffel et al. 2007). Fig. 14 presents a histogram comparing the intermediate-age SP of the galaxies where CN was clearly detected (Riffel et al. 2007) and those with no detections in a visual inspection. The objects with a clear CN detection have contributions of the intermediate-age component higher than ∼20 per cent, with a mean value of 40 ± 15 per cent. Regarding the galaxies where CN was not detected, the values are biased to contributions lower than ∼30 per cent. The mean value derived for the intermediate age for the sources without CN detection is 27 ± 20 per cent.

In four galaxies where CN was not detected we obtained fractions of the x_I component higher than ∼35 per cent. This result may appear contradictory, as the CN band is the stellar feature that most suitably traces the intermediate-age component. For NGC 5728, for instance, we associate the 69 per cent of the intermediate-age component with our shorter spectral coverage (see Section 5.1.1) and the low signal-to-noise ratio (S/N). For ESO 428-G014, Mrk 1210 and MCG 5-13-17, the CN band is totally filled by the Paγ emission line (fig. 2 of Riffel et al. 2006).

We conclude this section arguing that our NIR spectral fitting confirms that the detection of the CN band in the spectrum of a galaxy can be taken as unambiguous evidence of the presence of an intermediate-age SP.

5.2 The featureless component

As discussed in Section 4.1, it is very difficult to distinguish a reddened young starburst from a $F_\nu \propto \nu^{-1.5}$ power law. However, this effect is even harder in the optical, where the main difference between a 5 Myr SSP and an FC seen through an absorption $A_v \sim$ 2–3 mag by dust is the presence of the Balmer absorption lines and Balmer jump in the blue side in the former (CF04).

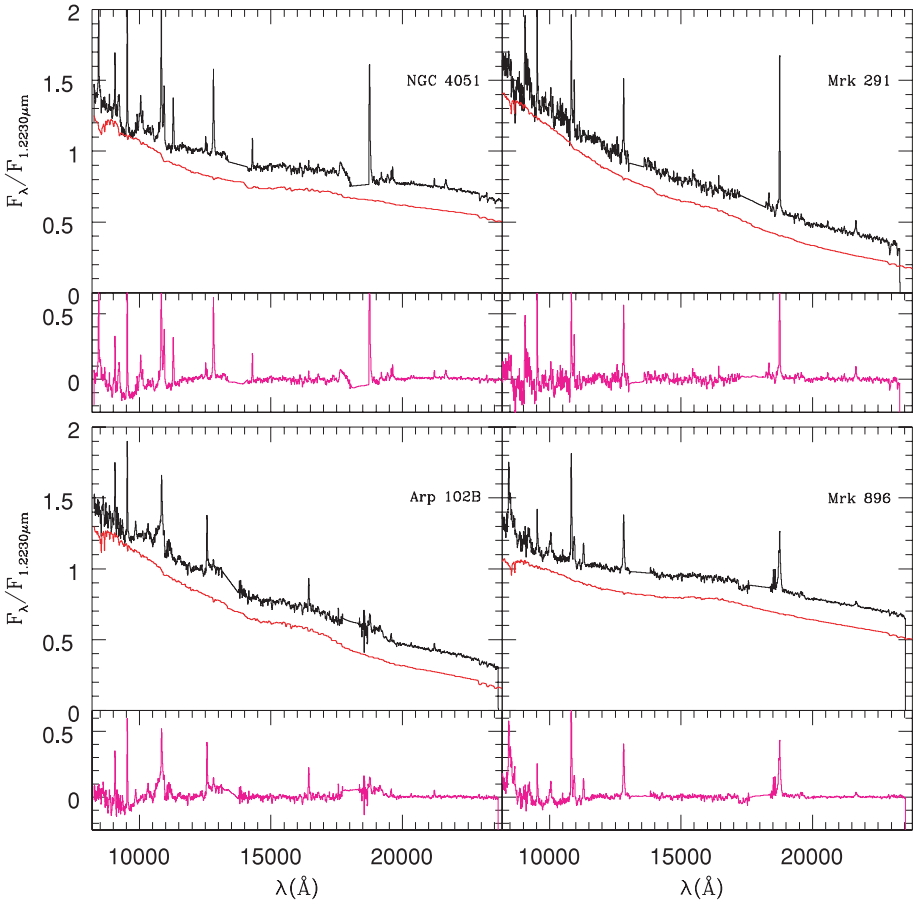

Figure 9. Same as Fig. 4.

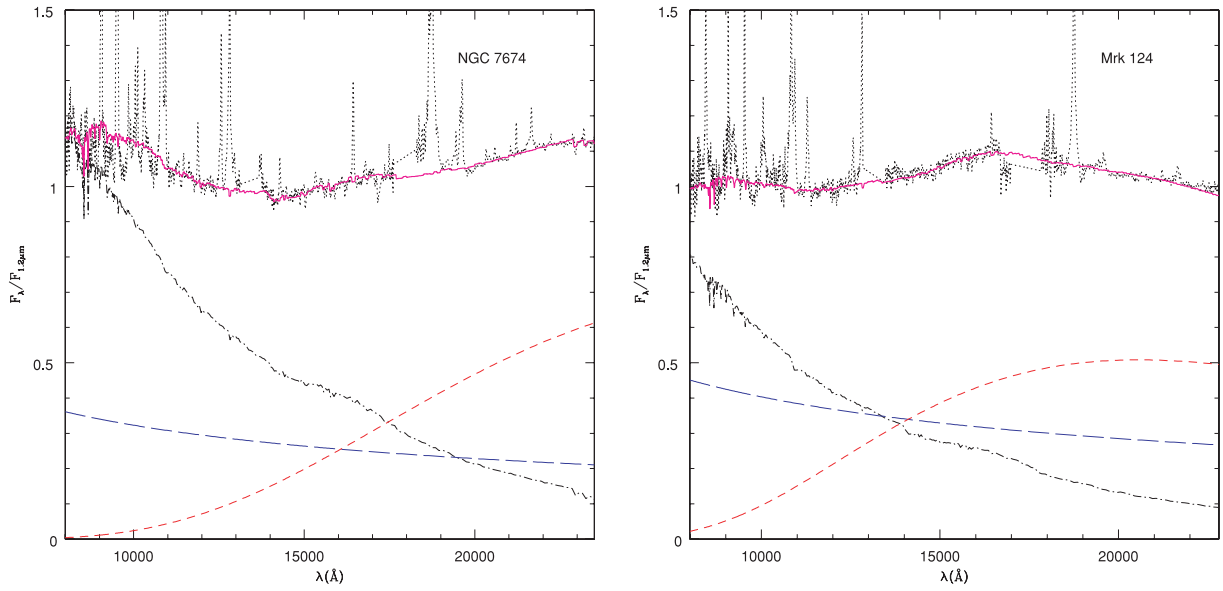

Figure 10. Three continuum components of NGC 7674 and Mrk 124. Dot-short-dashed line represents the SP ($x_y + x_I + x_o$). The FC and hot dust component are represented by the long and short dashed lines, respectively. The solid line is the sum of the three components and the dotted line represents the observed spectrum.

Cid Fernandes & Terlevich (1995) predicted that a broad component in Hβ becomes distinguishable whenever the scattered FC contributes with $\geq$20 per cent to the optical continuum light. With our synthesis we can investigate this issue in the NIR. Six out of 15 Sy 2 galaxies of our sample display an FC contribution higher than $\gtrsim$20 per cent (Table 3). Interestingly, a broad component in the hydrogen lines is detected in the spectra of the six sources: Mrk 1066 (e.g. Veilleux, Goodrich & Hill 1997), Mrk 573 (Nagao et al.

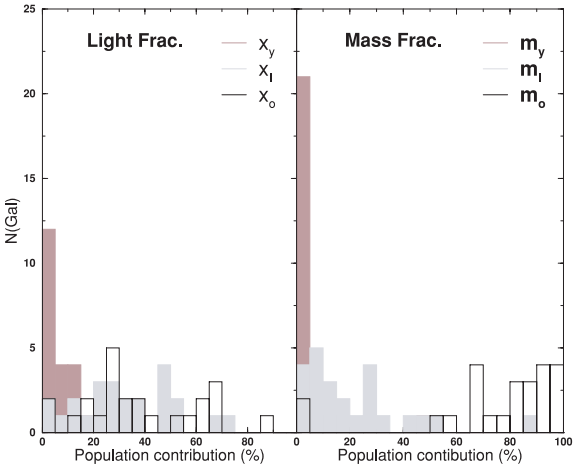

Figure 11. Histograms comparing the population vector components. Light-weighted at the left-hand panel and mass-weighted to the right-hand one. The lines (colours) indicating each component of $\boldsymbol{v}$ are on the labels.

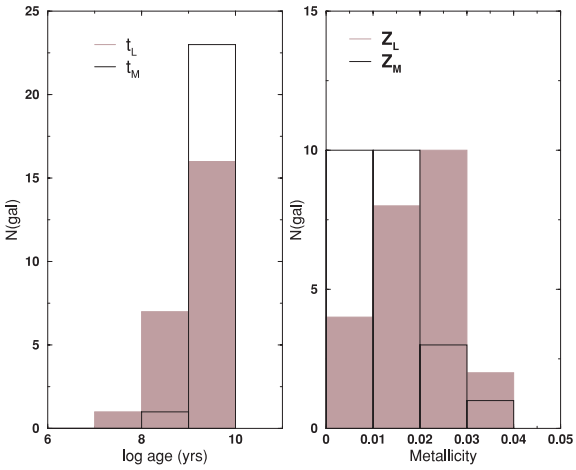

Figure 12. Histograms comparing our results in terms of light and mass fractions. At left we show a histogram of light- (filled) and mass-weighted (solid line) mean ages. At the right we present a histogram comparing the light (filled) and mass-weighted mean metallicities.

2004), NGC 1275 (e.g. Ho et al. 1997), NGC 2110 (e.g. Reunanen, Kotilainen & Prieto 2003), NGC 262 (e.g. Miller & Goodrich 1990) and NGC 7674 (e.g. Miller & Goodrich 1990).

For two of our galaxies a broad component is reported in the literature, and we do not detect strong contribution of the FC component. The first one is Mrk 1210, where a broad component of Hα and Hβ is detected in polarized light (Tran, Miller & Kay 1992; Tran 1995) and in the NIR HI lines (Mazzalay & Rodríguez-Ardila 2007) for which we find a ∼12 per cent contribution of the FC component and $x_{\rm Y} \sim 10$ per cent. Our NIR synthesis for this galaxy is consistent with that obtained by CF04 in the optical, but we tend to find a lower contribution of the young component. The second object is NGC 5953, where Gonçalves, Véron-Cetty & Véron (1999) report the possible detection of a very weak broad Hα line, but we did not find any contributions of FC and $x_{\rm Y}$. CF04 report a contribution of 18 per cent for the non-thermal component. No broad components are detected in our NIR spectrum (see Riffel et al. 2006).

The minimum FC contribution predicted by Cid Fernandes & Terlevich (1995) seems to be reflected in the NIR, as we clearly detect FC fractions higher than 20 per cent in the Sy 2 objects with

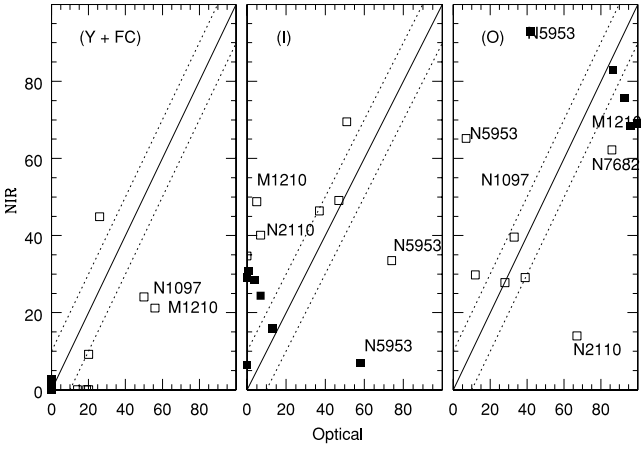

Figure 13. Comparison of the population vectors obtained in the NIR (this work) and in the optical (CF04) for seven objects in common. The symbols indicate the population vectors. The full line is the identity line; the dotted lines represent ±10 per cent deviation from the identity. Open and filled symbols are the flux and mass fraction, respectively.

a broad component in the HI lines. Therefore, our results reinforce their predictions. In addition, we detect FC >20 per cent in almost all Sy 1 sources,[11] which is consistent with the above arguments. However in four of our Sy 1 galaxies (Mrk 291, Arp 102 B, MCG-5-13-17 and NGC 1097) we detect fractions of FC < 20 per cent. For the first three objects we associate this ambiguity with the absence of features suitable to properly fit the absorption spectra and to a poor S/N in the blue side of the spectrum (see below). As discussed by CF04 and CF05, a high S/N is required for an adequate detection of the different contributions to the integrated spectra. Interestingly, the three objects display the presence of hot dust, which is in full agreement with the nature of the Sy 1 objects predicted by the unified model for AGN (see Section 5.3). NGC 1097, originally classified as LINER on the basis of its optical spectrum (Keel 1983), was reclassified by Storchi-Bergmann, Baldwin & Wilson (1993), Storchi-Bergmann et al. (1997) and Storchi-Bergmann et al. (2003) as a Sy 1 after observing broad Balmer emission lines, a featureless blue continuum and double peak profiles. Our spectral synthesis for NGC 1097 agrees with that obtained by CF04. Moreover, our value of $x_{\rm Y} \sim 20$ per cent is consistent with the starburst nature of this galaxy (Storchi-Bergmann et al. 2005).

It is worthwhile to mention at this point that the $W_{\rm CaT}$ values, measured for almost all objects of our sample (see Section 3), even if the dilution is considered, are consistent with values measured in normal spiral galaxies ($\lesssim$15 Å; Bica & Alloin 1987). However, in two cases, NGC 262 and NGC 2110, if we account for the dilution we reach very high values for $W_{\rm CaT}$ (∼17 and ∼25 Å, respectively). One explanation is that the $W_{\rm CaT}$ of these sources is overestimated due to the effects on the continuum and absorption lines by telluric features (see Table 1). Other possibility lies in the fact that the FC component is more sensitive to shorter wavelengths ($\lambda \lesssim 10\,000$ Å; see Fig. 10), which is our region with the lower number of constraints[12] and the lower S/N (the border of the spectrum; $\lambda \leq$ 9000 Å). Therefore, the FC component can be overestimated in these sources.

[11] With a mean value of ∼20 per cent if all Sy 1 sources are considered and ∼32 per cent if we exclude Mrk 291, Arp102B, MCG-5-13-17 and NGC 1097.

[12] Due to the large number of emission lines which are masked out.

Table 4. Dust properties for our galaxy sample.

T(K)	$L^{\rm gr}_{\nu,\rm ir}$(a)		Seyfert 2 NGC 262	NGC 2110	Mrk 1210	Mrk 1275	NGC 7674	Seyfert 1 Mrk 334	MCG 5-13-17	Mrk 124	NGC 3227	NGC 4051	Mrk 291	Arp 102 B	Mrk 896
		Cont. (per cent)	0	0	0.5	0.3	0	0	0	0	0	0	0	0	0
		$F_{\rm BB}$ (b)			7.53	10.79									
800	15.08	$L_{\rm BB}$ (c)			2.62	6.36									
		$N_{\rm gr}$ (d)			173.76	421.51									
		$M_{\rm HD}$ (e)			103.33	250.65									
		Cont. (per cent)	1.8	0	0	0	2.2	0	0	0	0	0	0	0	0
		$F_{\rm BB}$ (b)	10.51				12.17								
900	25.93	$L_{\rm BB}$ (c)	4.54				19.46								
		$N_{\rm gr}$ (d)	175.21				750.60								
		$M_{\rm HD}$ (e)	104.19				446.34								
		Cont. (per cent)	0	0	0	0	0	0	0	0	0	2.3	0	0	0
		$F_{\rm BB}$ (b)										7.12			
1200	97.39	$L_{\rm BB}$ (c)										0.07			
		$N_{\rm gr}$ (d)										0.76			
		$M_{\rm HD}$ (e)										0.45			
		Cont. (per cent)	0	0	0	0	5.7	0	0	0	0	2.0	0	0	0
		$F_{\rm BB}$ (b)					2.54					4.05			
1300	140.75	$L_{\rm BB}$ (c)					4.07					0.04			
		$N_{\rm gr}$ (d)					28.91					0.30			
		$M_{\rm HD}$ (e)					17.19					0.18			
		Cont. (per cent)	3.6	0.9	0	0	0	8.2	3.9	22.6	2.1	2.5	4.5	3.0	13.7
		$F_{\rm BB}$ (b)	1.21	1.07				5.17	3.70	6.54	4.35	3.61	0.56	1.13	6.29
1400	197.92	$L_{\rm BB}$ (c)	0.52	0.12				4.76	1.10	39.64	0.12	0.04	1.32	1.26	8.39
		$N_{\rm gr}$ (d)	2.64	0.63				24.04	5.54	200.31	0.63	0.19	6.66	6.36	42.42
		$M_{\rm HD}$ (e)	1.57	0.37				14.29	3.29	119.11	0.37	0.11	3.96	3.78	25.22
$\sum M_{\rm HD}$ (e)			106	0.37	103	251	463	14	3	119	0.4	0.75	4	4	25
cz (f)			4507	2335	4046	4046	8671	6579	3731	16878	1157	700	10552	700	7922

Notes. (a) 1×10^{-19} erg s^{-1} Hz^{-1}; (b) 1×10^{-27} erg cm^{-2} s^{-1} Hz^{-1}; (c) 1×10^{-27} erg s^{-1} Hz^{-1}; (d) 1×10^{43}; (e) 1×10^{-5} M$_{\odot}$; (f) From NED. Note that as we have not detected contributions for the $T =$ 700 K, 2.64 and $T = 1100$ K BB components we left them out from the table.

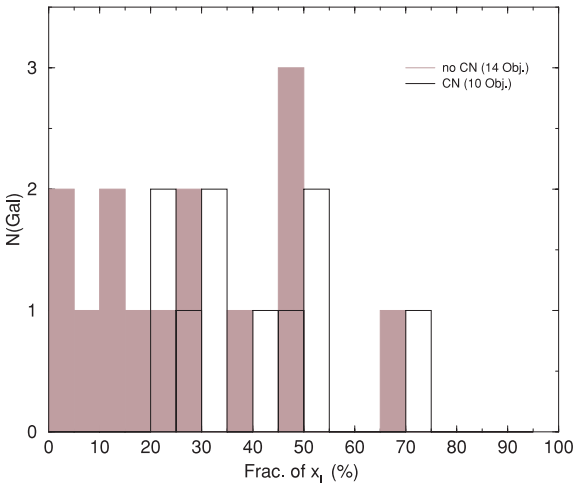

Figure 14. Histograms comparing the intermediate-age component of the galaxies with CN detection (empty histogram) and un-detection (shaded).

5.3 Dust emission

A rapid look at Column 5 of Table 3 shows an excess of emission over the SP and the FC for half of the AGN spectra. This excess (see Fig. 10), characterized by a Planck distribution, suggests emission from hot dust grains. Since Barvainis (1987), evidence of the presence of dust near the sublimation temperature has been observed in the central region of AGNs (e.g. Marco & Alloin 1998, 2000; Rodríguez-Ardila, Contini & Viegas 2005; Rodríguez-Ardila & Mazzalay 2006; Riffel et al. 2009). In order to quantify the dust contribution, we show in Table 4 the individual contribution of each blackbody over the temperature interval 800–1400 K. Note that as the $T = 700$ K and $T = 1000$ K components were not detected, we dropped them from Table 4.

Only in five Sy 2 galaxies we have detected hot dust, while a positive detection is reported for all Sy 1s. The obvious reason for this is that we are dealing with hot dust in the K band ($T \sim 1000$ K), and in the case of Sy 2s the dust is cooler ($T \sim 600$ K), thus more visible in the L or M bands. This hypothesis is supported by the fact that in two Sy 1 galaxies, Mrk 1239 and Mrk 766, we can see directly the presence of hot dust in the K band (Rodríguez-Ardila et al. 2005; Rodríguez-Ardila & Mazzalay 2006). There are two remarkable cases, Mrk 573 and Mrk 1066, where we have detected a significant fraction of the FC component and no hot dust. There are some possible explanations for this, the first two are those discussed above. Another possibility is that at least a significant fraction of the detected FC component is due to a very young starburst ($t \lesssim 5$ Myr). The latter, as discussed above (see Section 5.2), lies in the fact that the FC can be overestimated due the small number of constraints in the shorter wavelengths.

The two main constituents of interstellar dust are graphite (carbon) and silicate grains (e.g. Krüegel 2003). As discussed in Section 5, the evaporation temperatures of graphite and silicate grains are 1500 K and ∼1000 K, respectively (Barvainis 1987; Granato & Danese 1994). The temperature derived for the BB component of almost all objects is ≥900 K (see BB_c and BB_h in Table 3), suggesting that hot dust close to the central source is probably composed by graphite grains instead of silicates. The only discrepant objects are Mrk 1210 and NGC 1275 with $T = 800$ K. Considering, however, that the spatial resolution in those objects is ∼400 pc (Riffel et al. 2006) and that the dust temperature is a function of the distance to the central source (Marco & Alloin 1998), it is very likely that dust at higher temperatures exists closer to the central source. This would rule out the possibility of silicates as the main component of the nuclear dust grains.

Table 5. Hot dust masses found in AGNs.

Galaxy	M_{HD} ($M_\odot$)	Spectra	Reference
NGC 7582	2.8×10^{-3}	Yes	Riffel et al. (2009)
Mrk 1239	2.7×10^{-2}	Yes	Rodríguez-Ardila & Mazzalay (2006)
Mrk 766	2.1×10^{-3}	Yes	Rodríguez-Ardila et al. (2005)
NGC 1068	1.1×10^{-3}	No	Marco & Alloin (2000)
NGC 7469	5.2×10^{-2}	No	Marco & Alloin (1998)
NGC 4593	5.0×10^{-4}	No	Santos-Lléo et al. (1995)
NGC 3783	2.5×10^{-3}	No	Glass (1992)
NGC 1566	7.0×10^{-4}	No	Baribaud et al. (1992)
Fairall 9	2.0×10^{-2}	No	Clavel, Wamsteker & Glass (1989)

Assuming that the temperature of the different BB found for each galaxy represents the distribution of temperatures for graphite grains in the nuclear region, we can estimate the lower limit of the hot dust mass responsible for the observed K-band excess (see Fig. 10) following the approach developed by Barvainis (1987).

The infrared spectral luminosity of each dust grain can be obtained from (Barvainis 1987)

$$L^{gr}_{\nu,ir} = 4\pi^2 a^2 Q_\nu B_\nu(T_{gr}) \ [\mathrm{erg\,s^{-1}\,Hz^{-1}}], \quad (8)$$

where a is the grain radius, $Q_\nu = q_{ir}\,\nu^\gamma$ is its absorption efficiency and $B_\nu(T_{gr})$ is the Planck function for a grain at temperature T_{gr}. $L^{gr}_{\nu,ir}$ was calculated assuming a typical grain radius $a = 0.05$ μm (Barvainis 1987; Kishimoto et al. 2007) $q_{ir} = 1.4 \times 10^{-24}$ and $\gamma = 1.6$ (Barvainis 1987). The values of $L^{gr}_{\nu,ir}$ are shown in Table 4.

The hot dust mass, M_{HD}, can be obtained by the equation (Rodríguez-Ardila et al. 2005)

$$M_{HD} \approxeq \frac{4\pi}{3} a^3 N_{HD} \rho_{gr}, \quad (9)$$

where $N_{HD} \approxeq \frac{L^{HD}_{ir}}{L^{gr}_{\nu,ir}}$ is the number of hot dust grains and ρ_{gr} is the density of the grain. L^{HD}_{ir} is the total NIR luminosity due to hot dust. It can be derived from the integrated the flux of each BB contribution over the spectral range between 0.01 and 160 μm found on each galaxy.[13] Then, we multiplied the integrated normalized flux by the actual flux at 1.2 μm (our normalization point) and convert it to the adequate units (from $\mathrm{erg\,cm^{-2}\,s^{-1}\,\AA^{-1}}$ to $\mathrm{erg\,cm^{-2}\,s^{-1}\,Hz^{-1}}$). The final result of this process is the flux of each BB contribution (F_{BB}). The values derived for our sample are presented in Table 4. The L^{HD}_{ir} was estimated using F_{BB} and cz listed in Table 4 (we have adopted $H_0 = 75\ \mathrm{km\,s^{-1}\,Mpc^{-1}}$).

Finally, we have estimated the lower limit for hot dust mass, for graphite grains with $\rho_{gr} = 2.26\ \mathrm{g\,cm^{-3}}$ (Granato & Danese 1994) and using equation (9). The hot dust mass of each BB distribution, as well as the total hot dust mass ($\sum M_{HD}$), is presented in Table 4.

To compare the mass values derived for our sample and those reported by other authors, Table 5 lists the masses available in the literature, determined following Barvainis (1987). It is important to note that only three objects, Mrk 1239, Mrk 766 and NGC 7582, of the nine listed in Table 5 have the hot dust mass estimated by means of spectroscopy. In the remaining six, the masses were determined using photometry. The spectroscopic approach allows a careful subtraction of the power-law contribution and the SP. Moreover, our

[13] Note that we have weighted the distribution according to its contribution to the total SED.

results have the advantage, over previous determinations, of considering the SP, the FC and the BB in the same fitting process. Thus, our study has increased significantly the number of AGNs with the mass of hot dust estimated.

Given that the radius of the integrated region covered by most of our data is less than ∼500 pc,[14] this value sets an upper limit to the size of the hot dust emission region. We may further constrain this emission region if we consider that in half of our sample the spatial resolution is $\lesssim$400 pc. It means that the bulk of the hot dust is more likely concentrated close to the central source.

The origin of the hot dust can be the putative torus required by the unified model for AGNs (Antonucci & Miller 1985; Antonucci 1993), which is a natural dust reservoir. This hypothesis is further supported by the detection of hot dust in the inner ∼25 pc of NGC 7582 (Riffel et al. 2009) and by Jaffe et al. (2004), who studied the mid-infrared spectrum of NGC 1068, using interferometry with the *Very Large Telescope Interferometer* (VLTI). The latter work shows that the 10 μm emission is due to hot dust at 800 K concentrated in the central pc of this object, surrounded by cooler dust ($T = 300$ K) in scales of ∼2–4 pc. However, the detailed discussion of dust distribution around the central region of AGNs is beyond the scope of this paper and is left for a forthcoming work (Riffel et al., in preparation).

6 FINAL REMARKS

In this work we investigate the NIR spectra of 24 Seyfert galaxies (nine Sy 1 and 15 Sy 2) observed with the IRTF SpeX, obtained in the short cross-dispersed mode. Our main focus was the SP, AGN FC and dust contribution properties, along the full wavelength coverage (0.8 μm–2.4 μm). We have analysed the absorption features located in the NIR. The approach followed here is based on the STARLIGHT code, which considers the whole observed spectrum, continuum and absorption features. This is the first instance where STARLIGHT is applied to this wavelength range. Besides, in this work we also consider for the first time hot dust as an additional element base.

The main results can be summarized as follows. We found evidence of correlation among the W_λ of Si I 1.59 μm × Mg I 1.58 μm, equally for both kinds of activity. Part of the $W_{\rm Na\,I\,2.21\,\mu m}$ and $W_{\rm CO\,2.3\,\mu m}$ strengths and the correlation between $W_{\rm Na\,I\,2.21\,\mu m}$ and $W_{\rm Mg\,I\,1.58\,\mu m}$ appear to be accounted for by galaxy inclination. For the seven objects in common with previous optical studies (based on the same method of analyses), the NIR SP synthesis does not reproduce well the optical results. Our synthesis shows significant differences between Sy 1 and Sy 2 galaxies. The hot dust component is required to fit the *K*-band spectra of ∼80 per cent of the Sy 1 galaxies, and only of ∼40 per cent of the Sy 2. Besides, about 50 per cent of the Sy 2 galaxies require a featureless component contribution in excess of 20 per cent, while this fraction increases to about 60 per cent in the Sy 1. Also, in about 50 per cent of the Sy 2, the combined FC and $X_{\rm Y}$ components contribute with more than 20 per cent, while this occurs in 90 per cent of the Sy 1. This suggests recent star formation (CF05) in the central region of our galaxy sample. We found that the light at 1.223 μm in central regions of the galaxies studied here contains a substantial fraction of intermediate-age SPs with a mean metallicity near solar. Moreover, our analysis confirms that the 1.1 μm CN band can be taken as an unambiguous tracer of intermediate-age SPs.

[14] Except for Arp 102 B, Mrk 124 and Mrk 291.

One consequence of this work – especially because of the simultaneous fitting of SP, FC and hot dust components, allowing a proper analysis of each one of them – is a 150 per cent (400 per cent if only spectroscopic studies are considered) increase in the number of AGNs with hot dust detected and the mass estimated.

What emerges from this work is that the NIR may be taken as an excellent window to study the SP of Sy 1 galaxies, as opposed to the usually heavily attenuated optical range. Our approach opens a new way to investigate and quantify the contribution of the three most important NIR continuum components observed in AGNs.

ACKNOWLEDGMENTS

We thank the anonymous referee for useful comments. R.R. thanks the Brazilian funding agency CAPES. A.R.A. acknowledges the support of the Brazilian Funding Agency CNPq under grant 311476/2006-6. The STARLIGHT project is supported by the Brazilian agencies CNPq, CAPES and FAPESP and by the France–Brazil CAPES/Cofecub program. This research has made use of the NASA/IPAC Extragalactic Data base (NED) which is operated by the Jet Propulsion Laboratory, California Institute of Technology, under contract with the National Aeronautics and Space Administration. We acknowledge the usage of the HyperLeda data base (http://leda.univ-lyon1.fr).

REFERENCES

Allard E. L., Knapen J. H., Peletier R. F., Sarzi M., 2006, MNRAS, 371, 1087
Antonucci R., 1993, ARA&A, 31, 473
Antonucci R. R. J., Miller J. S., 1985, ApJ, 297, 621
Asari N. V., Cid Fernandes R., Stasińska G., Torres-Papaqui J. P., Mateus A., Sodré L., Schoenell W., Gomes J. M., 2007, MNRAS, 381, 263
Baribaud T., Alloin D., Glass I., Pelat D., 1992, A&A, 256, 375
Barvainis R., 1987, ApJ, 320, 537
Bica E., 1988, A&A, 195, 9
Bica E., Alloin D., 1987, A&A, 186, 49
Bica E., Pastoriza M. G., da Silva L. A. L., Dottori H., Maia M., 1991, AJ, 102, 1702
Bonatto C., Pastoriza M. G., Alloin D., Bica E., 1998, A&A, 334, 439
Bonatto C., Bica E., Pastoriza M. G., Alloin D., 2000, A&A, 355, 99
Bruzual G., Charlot S., 2003, MNRAS, 344, 1000
Cardelli J. A., Clayton G. C., Mathis J. S., 1989, ApJ, 345, 245
Cenarro A. J., Cardiel N., Gorgas J., Peletier R. F., Vazdekis A., Prada F., 2001, MNRAS, 326, 959
Cid Fernandes R., 1997, Rev. Mex. Astron. Astrofis. Ser. Conf., 6, 201C
Cid Fernandes R. J., Terlevich R., 1995, MNRAS, 272, 423
Cid Fernandes R. J., Storchi-Bergmann T., Schmitt H. R., 1998, MNRAS, 297, 579
Cid Fernandes R., Gu Q., Melnick J., Terlevich E., Terlevich R., Kunth D., Rodrigues Lacerda R., Joguet B., 2004, MNRAS, 355, 273 (CF04)
Cid Fernandes R., Mateus A., Sodré L., Stasińska G., Gomes J. M., 2005a, MNRAS, 358, 363 (CF05)
Cid Fernandes R., González Delgado R. M., Storchi-Bergmann T., Martins L. Pires, Schmitt H., 2005b, MNRAS, 356, 270
Cid Fernandes R. et al., 2009, Rev. Mex. Astron. Astrofis. Ser. Conf., 35, 127
Clavel J., Wamsteker W., Glass I. S., 1989, ApJ, 337, 236
Davies R. I. et al., 2006, ApJ, 646, 754
Davies R. I., Mueller Sánchez F., Genzel R., Tacconi L. J., Hicks E. K. S., Friedrich S., Sternberg A., 2007, ApJ, 671, 1388
Davies R., Maciejewski W., Hicks E., Tacconi L., Genzel R., Engel H., 2009, preprint (arXiv:0903.0313)
Dors O. L., Jr, Storchi-Bergmann T., Riffel R. A., Schimdt, Alex. A., 2008, A&A, 482, 59

Engelbracht C. W., Rieke M. J., Rieke G. H., Kelly D. M., Achtermann J. M., 1998, ApJ, 505, 639
Fathi K., Storchi-Bergmann T., Riffel R. A., Winge C., Axon D. J., Robinson A., Capetti A., Marconi A., 2006, ApJ, 641, 25
Ferrarese L., Merritt D., 2000, ApJ, 539, L9
Filippenko A. V., Ho L. C., Sargent W. L. W., 1993, ApJ, 410, 75
Garcia-Rissmann A., Vega L. R., Asari N. V., Cid Fernandes R., Schmitt H., González Delgado R. M., Storchi-Bergmann T., 2005, MNRAS, 359, 765
Garcia-Vargas M. L., Diaz A. I., Terlevich R., Terlevich E., 1989, Ap&SS, 157, 125
Glass I., 1992, MNRAS, 256, 23P
Gonçalves A. C., Véron-Cetty M.-P., Véron P., 1999, A&AS, 135, 437
Gonzalez Delgado R. M., Heckman T., Leitherer C., Meurer G., Krolik J., Wilson A.S., Kinney A., Koratkar A., 1998a, ApJ, 505, 174
González Delgado R. M., Leitherer C., Heckman T., Lowenthal J. D., Ferguson H. C., Robert C., 1998b, ApJ, 495, 698
González Delgado R. M., Heckman T., Leitherer C., 2001, ApJ, 546, 845
González Delgado R. M., Cid Fernandes R., Pèrez E., Martins L. P., Storchi-Bergmann T., Schmitt H., Heckman T., Leitherer C., 2004, ApJ, 605, 127
Granato G. L., Danese L., 1994, MNRAS, 268, 235
Heckman T. M., 2004, in Ho L. C. ed, Coevolution of Black Holes and Galaxies, from the Carnegie Observatories Centennial Symposia. Part of the Carnegie Observatories Astrophysics Series. Cambridge University Press, Cambridge, p. 358
Heckman T. M., Gonzalez-Delgado R. M., Leitherer C., Meurer G. R., Krolik J., Wilson A. S., Koratkar A., Kinney A., 1997, ApJ, 482, 114
Ho L. C., Filippenko A. V., Sargent W. L. W., Peng C. Y., 1997, ApJS, 112, 391
Hunt L. K., Thuan T. X., Izotov Y. I., 2003, ApJ, 588, 281
Iben I., Jr, Renzini A., 1983, ARA&A, 21, 271
Imanishi M., 2002, ApJ, 569, 44
Imanishi M., Dudley C. C., 2000, ApJ, 545, 701
Jaffe W. et al., 2004, Nat, 429, 47J
Joguet B., Kunth D., Melnick J., Terlevich R., Terlevich E., 2001, A&A, 380, 19
Keel W. C., 1983, ApJ, 269, 466
Knapen J. H., Shlosman I., Peletier R. F., 2000, ApJ, 529, 93
Koski A. T., 1978, ApJ, 223, 56
Kishimoto M., Hönig S. F., Beckert T., Weigelt G., 2007, A&A, 476, 713
Krüegel E., 2003, The Physics of Interstellar Dust. IoP, Bristol
Lançon A., Wood P. R., 2000, A&AS, 146, 217
Lançon A., Goldader J. D., Leitherer C., González Delgado R. M., 2001, ApJ, 552, 150
Maiolino R., Ruiz M., Rieke G. H., Papadopoulos P., 1997, ApJ, 485, 552
Marco O., Alloin D., 1998, A&A, 336, 823
Marco O., Alloin D., 2000, A&A, 353, 465
Maraston C., 1998, MNRAS, 300, 872
Maraston C., 2005, MNRAS, 362, 799 (M05)
Marino A. F., Villanova S., Piotto G., Milone A. P., Momany Y., Bedin L. R., Medling A. M., 2008, A&A, 490, 625
Mateus A., Sodré L., Cid Fernandes R., Stasińska G., Schoenell W., Gomes J. M., 2006, MNRAS, 370, 721
Mazzalay X., Rodríguez-Ardila A., 2007, A&A, 463, 445
Miller J. S., Goodrich R. W., 1990, ApJ, 355, 456
Mizutani K., Suto H., Maihara T., 1994, ApJ, 421, 475
Moorwood A. F. M., Glass I. S., 1982, A&A, 115, 84
Nagao T., Kawabata K. S., Murayama T., Ohyama Y., Taniguchi Y., Shioya Y., Sumiya R., Sasaki S. S., 2004, AJ, 128, 2066
Norman C., Scoville N., 1988, ApJ, 332, 124
Oliva E., Origlia L., Kotilainen J. K., Moorwood A. F. M., 1995, A&A, 301, 55
Origlia L., Oliva E., 2000, New Astron. Rev., 44, 257
Origlia L., Moorwood A. F. M., Oliva E., 1993, A&A, 280, 536
Paturel G., Petit C., Prugniel P., Theureau G., Rousseau J., Brouty M., Dubois P., Cambrésy L., 2003, A&A, 412, 45
Pogge R. W., 1989, ApJS, 71, 433
Raimann D., Storchi-Bergmann T., González Delgado R. M., Cid Fernandes R., Heckman T., Leitherer C., Schmitt H., 2003, MNRAS, 339, 772
Ramos Almeida C., Pérez García A. M., Acosta-Pulido J. A., 2009, ApJ, 694, 1379
Rayner J. T., Toomey D. W., Onaka P. M., Denault A. J., Stahlberger W. E., Vacca W. D., Cushing M. C., Wang S., 2003, PASP, 155, 362
Reunanen J., Kotilainen J. K., Prieto M. A., 2003, MNRAS, 343, 192
Rieke G. H., Lebofsky M. J., Thompson R. I., Low F. J., Tokunaga A. T., 1980, ApJ, 238, 24
Riffel R., Rodríguez-Ardila A., Pastoriza M. G., 2006, A&A, 457, 61
Riffel R., Pastoriza M. G., Rodríguez-Ardila A., Maraston C., 2007, ApJ, 659, L103
Riffel R., Rogemar A., Storchi-Bergmann T., Winge C., McGregor P. J., Beck T., Schmitt H., 2008a, MNRAS, 385, 1129
Riffel R., Pastoriza M. G., Rodríguez-Ardila A., Maraston C., 2008b, MNRAS, 388, 803
Riffel R. A., Storchi-Bergmann T., Dors O. L., Jr, Winge C., 2009, MNRAS, 393, 783
Rodríguez-Ardila A., Viegas S. M., 2003, MNRAS, 340, 33
Rodríguez-Ardila A., Mazzaly Z., 2006, MNRAS, 367, L57
Rodríguez-Ardila A., Contini M., Viegas S. M., 2005, MNRAS, 357, 220
Rudy R. J., Mazuk S., Puetter R. C., Hamann F., 2000, ApJ, 539, 166
Santos-Lléo M., Clavel J., Barr P., Glass I. S., Pelat D., Peterson B. M., Reichert G., 1995, MNRAS, 274, 1
Sarzi M., Rix H. W., Shields J. C., Ho L. C., Barth A. J., Rudnick G., Filippenko A. V., Sargent W. L. W., 2005, ApJ, 628, 169
Sarzi M., Allard E. L., Knapen J. H., Mazzuca L. M., 2007, MNRAS, 380, 949
Schmidt A. A., Copetti M. V. F., Alloin D., Jablonka P., 1991, MNRAS, 249, 766
Schmitt H. R., Bica E., Pastoriza M. G., 1996, MNRAS, 278, 965
Schmitt H. R., Storchi-Bergmann T., Cid Fernandes R., 1999, MNRAS, 303, 173
Shields J. C. et al., 2007, ApJ, 654, 125
Shlosman I., Frank J., Begelman M. C., 1989, Nat, 338, 45
Shlosman I., Begelman M. C., Frank J., 1990, Nat, 345, 679
Storchi-Bergmann T., Baldwin J. A., Wilson A. S., 1993, ApJ, 410, L11
Storchi-Bergmann T., Eracleous M., Ruiz M. T., Livio M., Wilson A. S., Filippenko A. V., 1997, ApJ, 489, 87
Storchi-Bergmann T., Raimann D., Bica E. L. D., Fraquelli H. A., 2000, ApJ, 544, 747
Storchi-Bergmann T. et al., 2003, ApJ, 598, 956
Storchi-Bergmann T., Nemmen R. S., Spinelli P. F., Eracleous M., Wilson A. S., Filippenko A. V., Livio M., 2005, ApJ, 624, L13
Terlevich E., Diaz A. I., Terlevich R., 1990, MNRAS, 242, 271
Thompson R. I., 1995, ApJ, 445, 700
Tokunaga A. T., Sellgren K., Smith R. G., Nagata T., Sakata A., Nakada Y., 1991, ApJ, 380, 452
Tran H. D., 1995, ApJ, 440, 578
Tran H. D., Miller J. S., Kay L. E., 1992, ApJ, 397, 452
Vega L. R., Asari N. V., Cid Fernandes R., Garcia-Rissmann A., Storchi-Bergmann T., González Delgado R. M., Schmitt H., 2009, MNRAS, 393, 846
Veilleux S., 2001, in Tacconi L., Lutz D., eds. Starburst Galaxies: Near and Far. Proceedings of a Workshop held at Ringberg Castle, Germany. Springer-Verlag, Heidelberg, p. 88
Veilleux S., Goodrich R. W., Hill G. J., 1997, ApJ, 477, 631

This paper has been typeset from a TEX/LATEX file prepared by the author.